Cellular/Molecular

The Active Zone Protein Family ELKS Supports Ca^{2+} Influx at Nerve Terminals of Inhibitory Hippocampal Neurons

Changliang Liu,[1] Lydia S. Bickford,[1]* Richard G. Held,[1]* Hajnalka Nyitrai,[1]* Thomas C. Südhof,[2,3] and Pascal S. Kaeser[1,2]

[1]Department of Neurobiology, Harvard Medical School, Boston, Massachusetts 02115, and [2]Department of Molecular and Cellular Physiology and [3]Howard Hughes Medical Institute, Stanford University, Stanford, California 94305

In a presynaptic nerve terminal, synaptic vesicle exocytosis is restricted to specialized sites called active zones. At these sites, neurotransmitter release is determined by the number of releasable vesicles and their probability of release. Proteins at the active zone set these parameters by controlling the presynaptic Ca^{2+} signal, and through docking and priming of synaptic vesicles. Vertebrate ELKS proteins are enriched at presynaptic active zones, but their functions are not well understood. ELKS proteins are produced by two genes in vertebrates, and each gene contributes ~50% to total brain ELKS. We generated knock-out mice for ELKS1 and found that its constitutive removal causes lethality. To bypass lethality, and to circumvent redundancy between ELKS1 and ELKS2 in synaptic transmission, we used a conditional genetic approach to remove both genes in cultured hippocampal neurons after synapses are established. Simultaneous removal of ELKS1 and ELKS2 resulted in a 50% decrease of neurotransmitter release at inhibitory synapses, paralleled by a reduction in release probability. Removal of ELKS did not affect synapse numbers or their electron microscopic appearance. Using Ca^{2+} imaging, we found that loss of ELKS caused a 30% reduction in single action potential-triggered Ca^{2+} influx in inhibitory nerve terminals, consistent with the deficits in synaptic transmission and release probability. Unlike deletion of the active zone proteins RIM, RIM-BP, or bruchpilot, ELKS removal did not lead to a measurable reduction in presynaptic Ca^{2+} channel levels. Our results reveal that ELKS is required for normal Ca^{2+} influx at nerve terminals of inhibitory hippocampal neurons.

Key words: **active zone; calcium; ELKS; knock-out; priming**

Introduction

In presynaptic nerve terminals, active zones are sites of neurotransmitter release that consist of a network of multidomain proteins anchored to the plasma membrane (Couteaux and Pécot-Dechavassine, 1970; Harlow et al., 2001; Südhof, 2012). At the active zone, the number of vesicles in the readily releasable pool (RRP) and the probability of release (p) of these vesicles are tightly controlled (Ariel and Ryan, 2012; Kaeser and Regehr, 2014). Proteins specifically localized to active zones include Rab3-interacting molecules (RIMs), Munc13s, ELKS (protein rich in the amino acids E, L, K, and S), Liprin-α, RIM-binding proteins (RIM-BPs), and piccolo/bassoon (Kaeser, 2011; Gundelfinger and Fejtova, 2012). These proteins cooperate to provide molecular scaffolds for tethering synaptic vesicles, they render vesicles fusion-ready in a process referred to as priming, and they couple presynaptic Ca^{2+} channels to release sites (Augustin et al., 1999; Koushika et al., 2001; Kittel et al., 2006; Weimer et al., 2006; Gracheva et al., 2008; Deng et al., 2011; Han et al., 2011; Kaeser et al., 2011; Liu et al., 2011). How individual proteins cooperate in these functions is incompletely understood.

The roles of mammalian ELKS proteins are enigmatic, in part because no simultaneous removal of both ELKS genes, *ELKS1* and *ELKS2*, has been pursued. ELKS, originally described as a gene fused to RET (Nakata et al., 1999), is also called Rab6IP2 (Monier et al., 2002), CAST (Ohtsuka et al., 2002; Deguchi-Tawarada et al., 2004), and ERC (Wang et al., 2002). The nematode *Caenorhabditis elegans* expresses a homolog of ELKS that acts downstream of syd2/liprin-α during active zone assembly (Deken et al., 2005; Dai et al., 2006). *Drosophila melanogaster* expresses a related protein termed bruchpilot (brp) that consists of a conserved N terminus and a C-terminal half with no homologous sequences in vertebrates (Monier et al., 2002; Kittel et al., 2006; Wagh et al., 2006). Its coiled-coil structure suggests that ELKS operates as a scaffolding molecule (Ohtsuka et al., 2002). In support of a scaffolding function, knock-out (KO) of ELKS2α

Received March 12, 2014; revised June 29, 2014; accepted July 18, 2014.

Author contributions: C.L., T.C.S., and P.S.K. designed research; C.L., L.S.B., R.G.H., H.N., and P.S.K. performed research; P.S.K. contributed unpublished reagents/analytic tools; C.L., R.G.H., H.N., T.C.S., and P.S.K. analyzed data; C.L. and P.S.K. wrote the paper.

This work was supported by the Alice and Joseph E. Brooks Fund (fellowship) to C.L., National Institutes of Health Grants 1F31NS089077 to R.G.H., 5K01DA029044 and 1R01NS083898 to P.S.K., the Nancy Lurie Marks Foundation to P.S.K., the Lefler Foundation to P.S.K., and the Brain Research Foundation to P.S.K. We also acknowledge the Neurobiology Imaging facility, supported by National Institute of Neurological Disorders and Stroke P30 Core Center Grant NS072030, for instrument availability and consultation. We thank Han Ly for technical support, Dr. Xinran Liu for help with electronmicroscopic analyses, Dr. Robert Hammer for blastocyst injections of ES cells, Dr. Nils Brose for Munc13 antibodies, Dr. Lu Chen for providing a custom MATLAB template to analyze synaptic puncta, and Dr. Wade Regehr for insightful discussions and comments on the manuscript.

The authors declare no competing financial interests.

*L.S.B., R.G.H., and H.N. contributed equally to this work.

Correspondence should be addressed to either of the following: Dr. Thomas C. Südhof, Howard Hughes Medical Institute, Stanford University, Stanford, CA 94305, E-mail: tcs1@stanford.edu; or Dr. Pascal S. Kaeser, Department of Neurobiology, Harvard Medical School, Boston, MA 02115, E-mail: kaeser@hms.harvard.edu.

DOI:10.1523/JNEUROSCI.0999-14.2014

 0270-6474/14/3412289-15$15.00/0

(also called CAST) leads to reduced active zone size at ribbon synapses (tom Dieck et al., 2012). This is consistent with phenotypes observed in brp mutant flies, which lack T-bars and exhibit decreased neurotransmitter release at the neuromuscular junction (NMJ), walking deficits, and mislocalization of fluorescently tagged, overexpressed Ca^{2+} channels (Kittel et al., 2006; Wagh et al., 2006; Fouquet et al., 2009). In the mouse hippocampus, ELKS2α KO resulted in an increase in inhibitory synaptic transmission (Kaeser et al., 2009), compatible with the mild phenotype observed in *C. elegans* (Deken et al., 2005). A major shortcoming in the genetic experiments in vertebrates to date (Kaeser et al., 2009; tom Dieck et al., 2012) is that simultaneous removal of ELKS1 and ELKS2 has not been performed. We here overcome this limitation by generating conditional KO mice for ELKS1 and ELKS2. We find that genetic removal of ELKS1 and ELKS2 leads to reduced release probability at inhibitory hippocampal synapses due to reduced action potential-triggered presynaptic Ca^{2+} influx.

Materials and Methods

ELKS antibodies. ELKS antibodies used in this study are (for an overview of protein isoforms, see Fig. 4*D*): P224 (Wang et al., 2002; Kaeser et al., 2009), rabbit polyclonal antiserum, binds to all ELKS isoforms (ELKS1αB, ELKS1αA, ELKS1βB, ELKS1βA, ELKS2αB, ELKS2αA, ELKS2βB, ELKS2βA); 4790 (Wang et al., 2002; Kaeser et al., 2009), rabbit polyclonal antiserum, binds to ELKS-B isoforms (ELKS1αB, ELKS1βB, ELKS2αB, ELKS2βB); 4791 (Wang et al., 2002), rabbit polyclonal antiserum, binds to ELKS1A (ELKS1αA, ELKS1βA); U5004 (Wang et al., 2002; Kaeser et al., 2009), rabbit polyclonal antiserum, binds to ELKS2 isoforms (ELKS2αB, ELKS2αA, ELKS2βB, ELKS2βA); ELKS-30 (Sigma-Aldrich catalog #E4531, RRID:AB_2100013), mouse monoclonal antibody, binds to ELKS-α isoforms (ELKS1αB, ELKS1αA, ELKS2αB, ELKS2αA), and E-1 (Santa Cruz Biotechnology catalog #sc-365715, RRID:AB_10841908), mouse monoclonal antibody, binds to ELKS1α isoforms (ELKS1αB, ELKS1αA).

Generation of mutant mice. ELKS1 conditional KO mice were generated by homologous recombination using methods described previously (Kaeser et al., 2011). In an initial approach, a targeting vector containing a neomycin cassette (flanked by frt sites), a diphtheria toxin expressing cassette, a tetracysteine tag within the coding sequence of exon 3, and loxp sites surrounding the coding sequence of exon 3 (the first coding exon of the ELKS1 gene), was constructed, linearized, and transfected into R1 embryonic stem (ES) cells. Positive clones were identified by Southern blotting, and two clones were used for injection into 129/SV blastocysts to generate chimeric mice. The ELKS1^{nc} mice were established by germ line transmission of the mutant allele from the chimeric mice, the neomycin resistance cassette was removed by flp recombination (Dymecki, 1996) to produce the ELKS1$^{nc\text{-}KI}$ mice, and exon 3 was removed by cre recombination (O'Gorman et al., 1997) to generate the ELKS1$^{nc\text{-}KO}$ mice. No surviving homozygote offspring were obtained in the ELKS1^{nc}, ELKS1$^{nc\text{-}KI}$, and ELKS1$^{nc\text{-}KO}$ lines. We concluded that the gene targeting disrupted ELKS1 expression (hence nc = nonconditional), which in turn led to embryonic lethality, and we corrected the targeting strategy. We duplicated the neomycin cassette (flanked by frt sites) and moved it further into the intron, removed the tetracysteine tag and moved the 5′ loxp into a 5′ intron that is surrounded by 5′ untranslated region (5′ UTR) exons. This revised targeting construct (see Fig. 1*D*) was linearized and transfected into R1 ES cells. ES cell clones were screened for homologous recombination by Southern blotting with outside probes at the 5′ and 3′ ends. Three positive clones were injected into 129/SV blastocysts, and chimeric male offspring were bred to C57BL/6 mice. Germ line transmission was identified by coat color, PCR genotyping, and Southern blotting and resulted in the ELKS1^{mutant} allele. In the ELKS1^{floxed} mice, the neomycin resistance cassette has been removed by crossing the ELKS1^{mutant} mice to flp transgenic mice (Dymecki, 1996); and for constitutive removal of ELKS1, the mice were further crossed to transgenic mice expressing cre recombinase in the male germ line (O'Gorman et al., 1997), resulting in the ELKS1^{KO} mice. ELKS1^{floxed} mice were genotyped with oligonucleotide primers PK05181 (GAA CAAGTTTCAGGACAGCCAAGG) and PK05182 (CAGGTGATGAC AATCTGAAGGC) to obtain a 250 base pair (bp) wild-type band versus a 300 bp mutant band. ELKS1^{KO} mice were genotyped with two independent reactions: with oligonucleotide primers PK06198 (CTGTA GATGAAGATGGCCTTTACC) and PK06200 (GGATGAGAACACTT GGTCACTTCC) resulting in a 350 bp wild-type band, and with PK06198 and PK05182 for obtaining a 300 bp mutant band. The ELKS1$^{nc\text{-}KO}$ (RRID:IMSR_JAX:007854) and the corrected ELKS1^{floxed} (RRID:IMSR_JAX:015830) alleles were submitted to The Jackson Laboratory to make them available to the community.

Mouse breeding and survival analysis. All animal experiments were performed according to institutional guidelines at the University of Texas Southwestern Medical Center, Stanford University, and Harvard University. Survival analyses were performed by comparing the observed genotype distribution of offspring of heterozygote matings with the expected distribution based on Mendelian inheritance (Kaeser et al., 2008). The χ^2 test was used to determine whether the obtained offspring ratio was significantly different from the expected ratio. For generating the ELKS conditional double knock-out (cDKO) neurons, the newly generated ELKS1^{floxed} mice were crossed to the previously generated ELKS2^{floxed} mice (Kaeser et al., 2009, RRID:IMSR_JAX:015831), and the mice were maintained as double homozygote line.

Cell cultures and lentiviral infection. Primary mouse hippocampal cultures from newborn pups were generated as previously described (Ho et al., 2006; Kaeser et al., 2008; Kaeser et al., 2009; Kaeser et al., 2011). All lentiviruses were produced in HEK293T cells by Fugene or Ca^{2+}-phosphate transfection. Neurons were infected with viruses that express cre recombinase with enhanced nuclear localization or an inactive truncation mutant thereof (Kaeser et al., 2011). Cre was expressed under a human-synapsin promoter, except for electron microscopic analyses and quantitative Western blotting with ^{125}I-labeled secondary antibodies, for which the ubiquitin promoter was used. Neuronal cultures were infected with 125–250 μl of HEK cell supernatant at 3–5 d *in vitro* (DIV). Infection rates were monitored by a fluorescent tag attached to nuclear cre recombinase, and only cultures in which no noninfected cells were found were analyzed.

qRT-PCR. For comparison of mRNA levels across tissues, organs (brain, liver, lung, spleen, kidney, and heart) of three 7-week-old wild-type mice were harvested and flash-frozen. Total RNA was extracted by standard methods and quantified by spectrophotometry. One-step RT-PCR was performed with TaqMan Gene Expression Assays (Life Technologies) and the iScript Reverse Transcriptase (Bio-Rad). The following gene-expression assays were used: ELKS1 (assay ID: Mm00453569_m1, gene name: Erc1), ELKS2 (assay ID: Mm01209943_m1, gene name: Erc2), Munc13-1 (assay ID: Mm01340418_m1, gene name: Unc13a), Munc13-2 (assay ID: Mm01351419_m1, gene name: Unc13b), synapsin1 (assay ID: Mm00449772_m1, gene name: Syn1), and GAPDH (assay ID: Mm99999915_g1, gene name: Gapdh). Reactions were performed three times for all samples using 0.3 μg RNA per 20 μl reaction on a real-time PCR detection system. Data were analyzed by determining the cycle threshold values (C_T) relative to internal GAPDH levels. For comparison of mRNA expression levels in cultured control and cDKO neurons, DIV 14 cultures were washed with PBS and RNA extraction, purification, quantification, and probe-based qRT-PCR was performed the same way as described above. The following TaqMan gene-expression assays were used: synapsin1 (assay ID: Mm00449772_m1, gene: Syn1), $Ca_V1.3$ (ID: Mm01209919_m1, gene: cacna1d), $Ca_V2.1$ (ID: Mm00432190_m1, gene: cacna1a), $Ca_V2.2$ (ID: Mm01333678_m1, gene: cacna1b), $Ca_V2.3$ (ID: Mm00494444_m1, gene: cacna1e), $Ca_V\beta1$ (ID: Mm01306805_m1, gene: cacnB1), $Ca_V\beta2$ (ID: Mm00659092_m1, gene: cacnB2), $Ca_V\beta3$ (ID: Mm00432244_m1, gene: cacnB3), and $Ca_V\beta4$ (ID: Mm00521623_m1, gene: cacnB4). Reactions were performed in triplicates for three independent cultures, using ~10 ng of RNA in a 10 μl reaction volume. Relative expression ratios were expressed as $2^{-\Delta\Delta C_T}$, where $\Delta\Delta C_T = \Delta C_{TcDKO} - \Delta C_{Tcontrol}$, ΔC_T is the synapsin1 normalized value.

5′ RACE amplification. RNA was purified from ELKS cDKO and control cultures. 5′ RACE was performed as described previously (Kaeser et

al., 2008). ELKS1β was identified in both genotypes by use of a gene-specific primer PK11362 (GCAGCCCTTTGCTCCTTAGC) for generating cDNA and a nested primer PK11363 (TCAGCACCTCAATATG TTGC) together with a primer supplied with the kit for amplification, and was followed by sequencing of the PCR product. We identified cDNAs that start with a 5′ UTR that is part of exon 4 of the ELKS1 gene; the start codon is likely an alternative start codon within exon 4 but may also be further downstream.

Immunofluorescence stainings and confocal imaging of cultured neurons. Neurons were fixed in 4% PFA/PBS, permeabilized in 0.1% Triton X-100/3% BSA/PBS, and incubated in primary antibodies 3 h at room temperature or 4°C overnight. The following primary antibodies were used: E-1 (1:500, Santa Cruz Biotechnology catalog #sc-365715, RRID: AB_10841908), ELKS-30 (1:500, Sigma-Aldrich catalog #E4531, RRID: AB_2100013), mouse anti-GAD2 (1:500, Synaptic Systems catalog #198111, RRID:AB_2107894, also called GAD65), rabbit anti-MAP2 (1: 1000, Synaptic Systems catalog #188002, RRID:AB_2138183), guinea pig anti-VGluT1 (1:1000, Synaptic Systems catalog #135304, RRID: AB_887878), mouse anti-synapsin (1:1000, Synaptic Systems catalog #106001, RRID:AB_2200566), rabbit anti-synapsin (1:1000, E028) (Hosaka and Südhof, 1999), mouse anti-GAD1 (1:1000, Millipore catalog #MAB5406, RRID:AB_2278725, also called GAD67), rabbit anti-$Ca_V2.1$ (1:100, Alomone Labs catalog #ACC-001, RRID:AB_2039764), rabbit anti-$Ca_V\beta3$ (1:500, Alomone Labs catalog #ACC-008, RRID: AB_2039787), and rabbit anti-$Ca_V2.2$ (1:500, Alomone Labs, catalog #ACC-002, RRID:AB_2039766). Stainings with anti-$Ca_V2.2$ and anti-$Ca_V\beta3$ antibodies were performed with a modified staining protocol (permeabilized and blocked in 0.1% glycine, 0.3% Triton X-100/10% FBS/PBS, and stained in 3% FBS/PBS) as described previously (Lazarevic et al., 2011; Davydova et al., 2014). AlexaFluor-405, -488, -546, and -633-conjugated secondary antibodies were used for detection. Images were acquired on a Leica TCS2 or Olympus FV1000 confocal microscope with 60× oil-immersion objectives with 1.4 numerical aperture; the pinhole was set to one airy unit, and identical settings were applied to all samples within an experiment. Single confocal sections were analyzed in ImageJ software (National Institutes of Health) or a custom MATLAB template (MathWorks) obtained from Dr. Lu Chen. For quantitation of the synaptic levels of $Ca_V2.1$, $Ca_V2.2$, and $Ca_V\beta3$ channels, GAD2 puncta were defined as the ROI, and the average intensity of $Ca_V2.1$, $Ca_V2.2$, and $Ca_V\beta3$ inside those ROIs was quantified. The intensity of $Ca_V2.1$, $Ca_V2.2$, and $Ca_V\beta3$ staining in cDKO neurons was normalized to the staining in control. All quantitative data are derived from ≥3 cultures; 3–10 fields of view were quantified per culture per genotype. The experimenter was blind to the genotype.

Quantitative Western blotting. Western blotting was performed according to standard protocols. For nonquantitative signal detection, chemiluminescence was used. For quantitation, secondary antibodies coupled to 125-iodine (^{125}I) were used (see Figs. 3 and 4), and intensity was quantified on a Storm PhosphorImager as described previously (Kaeser et al., 2008). Alternatively (see Fig. 9), fluorescently tagged antibodies were used for increased sensitivity according to the following protocol. Western blotting was performed on crude SDS-lysates of three batches of ELKS cDKO and control neurons grown on 12-well cultureplates at DIV 14. After SDS-PAGE, gels were transferred onto nitrocellulose membranes and blocked in 5% nonfat milk/5% goat serum. Membranes were incubated overnight at 4°C with primary antibodies. The following primary antibodies were used: rabbit anti-ELKS 4790 (1: 1000, see above), rabbit anti-liprin-$\alpha3$ (1:2000, 4396) (Schoch et al., 2002), rabbit anti-synapsin (1:500, E028) (Hosaka and Südhof, 1999), mouse anti-synapsin (1:2000, Synaptic Systems, catalog #106 001, RRID: AB_2200566), mouse anti-β-actin (1:3000, Sigma-Aldrich, catalog #A1978, RRID:AB_476692), rabbit anti-β-actin (1:500, GeneTex, catalog #GTX110564, RRID:AB_10618080), rabbit anti-$Ca_V2.1$; (1:400, Synaptic Systems, catalog #152 103, RRID:AB_2228389), rabbit anti-$Ca_V2.2$ (1:100, Alomone Labs, catalog #ACC-002, RRID:AB_2039766), rabbit anti-$Ca_V\beta3$ (1:200, Alomone Labs, catalog #ACC-008, RRID:AB_2039787), and mouse anti-$Ca_V\beta4$ (1:40, NeuroMab, catalog #73-054, RRID: AB_10671176). The following fluorescent secondary antibodies were used: donkey anti-mouse IRDye 800CW IgG (1:10,000, LI-COR, catalog #926-32212, RRID:AB_621847), donkey anti-rabbit IRDye 800CW IgG (1:10,000, LI-COR, catalog #926-32213, RRID:AB_621848), donkey anti-mouse IRDye 680RD IgG (1:10,000, LI-COR, catalog #926-32222, RRID:AB_621844), and donkey anti-rabbit IRDye 680RD IgG (1:10,000, LI-COR, catalog #926-32223, RRID:AB_621845). Each membrane was incubated with antibodies against the protein of interest and anti-synapsin antibodies as a loading control. Blots were scanned on a LI-COR Odyssey Fluorescent Scanner, and fluorescent images were analyzed in ImageJ Software. cDKO protein levels are expressed normalized to the average of the control condition.

Electrophysiology. Electrophysiological recordings in cultured hippocampal neurons were performed as described previously (Maximov et al., 2007; Kaeser et al., 2011) at DIV 14–18 at room temperature. The extracellular solution contained the following (in mM): 140 NaCl, 5 KCl, 2 $CaCl_2$, 2 $MgCl_2$, 10 HEPES-NaOH, pH 7.4, 10 glucose (~310 mOsm). The following drugs were added in the bath: for evoked IPSCs, APV (50 μM) and CNQX (20 μM); for miniature IPSC (mIPSCs) and RRP measurements, TTX (1 μM), APV (50 μM), and CNQX (20 μM). Glass pipettes for patch clamping were pulled at 2–4 MΩ and were filled with intracellular solution containing (in mM) the following: 120 CsCl, 5 NaCl, 10 EGTA, 1 $MgCl_2$, 10 sucrose, 10 HEPES-CsOH, pH 7.4, 4 Mg-ATP, 0.4 GTP (~300 mOsm). Cells were held at −70 mV. Cells were discarded if access resistance exceeded 15 MΩ or 20 MΩ during recording of evoked or spontaneous synaptic currents, respectively. Action potentials in presynaptic neurons were elicited with a focal stimulation electrode fabricated from nichrome wire. In this preparation, TTX entirely blocks synaptic transmission (IPSC amplitude in control: 4.32 ± 0.71 nA, with TTX: 0.02 ± 0.01 nA, $n = 10$ cells), indicating that all release is triggered by action potentials and not by passive conductances. For $[Ca^{2+}]_{ex}$ dependence of IPSC amplitudes, recordings started and ended at 2 mM $[Ca^{2+}]_{ex}$/2 mM $[Mg^{2+}]_{ex}$, and the neurons were perfused with solutions containing 0.5/3.5, 1/3, 2/2, 5/2, and 10/2 mM $[Ca^{2+}]_{ex}$ /$[Mg^{2+}]_{ex}$ in variable order. Amplitudes were plotted as a function of $[Ca^{2+}]_{ex}$ and fitted with the Hill equation ($I=I_{max}/1 + EC_{50}/[Ca^{2+}]_{ex})^n$) for each individual cell; no constraints were used for fitting. For $[Ca^{2+}]_{ex}$ dependence of mIPSC frequency, recordings were performed in solutions containing 0 mM $[Ca^{2+}]_{ex}$/4 mM $[Mg^{2+}]_{ex}$/1 mM EGTA, 0.5 mM $[Ca^{2+}]_{ex}$/3.5 mM $[Mg^{2+}]_{ex}$, or 2 mM $[Ca^{2+}]_{ex}$/2 mM $[Mg^{2+}]_{ex}$. mIPSC kinetics were determined for each cell by averaging the waveform of all events aligned to the beginning of the events. Rise times were measured as the time interval between 20% and 80% of the peak amplitude and decay τ as the interval from 100% to 37% of the decay phase. The RRP was measured by focal application of 0.5 M sucrose with a picospritzer for 30 s in the presence of TTX (1 μM). For action potential studies in 10 mM extracellular tetraethylammonium (TEA), neurons were filled with the following (in mM): 140 K Gluconate, 0.1 EGTA, 2 $MgCl_2$, 4 Na_2ATP, 1 NaGTP, and 10 HEPES-KOH (pH 7.4, ~300 mOsm). A minimal step current that was sufficient to evoke at least one action potential (100–300 pA for 500 ms) was injected, and only the first action potential evoked in each cell was used for analysis. Data were acquired with an Axon 700B Multiclamp amplifier using pClamp10. For all electrophysiological experiments, the experimenter was blind to the genotype throughout data acquisition and analysis.

Ca^{2+} imaging. All Ca^{2+} imaging experiments were done with hippocampal cultures infected with lentiviruses (expressing active cre or inactive cre) at DIV 5, and neurons were examined at DIV 15–18 in whole-cell patch-clamp configuration at room temperature. The extracellular solution contained the following (in mM): 140 NaCl, 5 KCl, 2 $CaCl_2$, 2 $MgCl_2$, 10 glucose, 0.05 APV, 0.02 CNQX, 0.05 PTX, 10 HEPES-NaOH (pH 7.4, ~310 mOsm). Glass pipettes were filled with intracellular solution containing the following (in mM): 140 K Gluconate, 0.1 EGTA, 2 $MgCl_2$, 4 Na_2ATP, 1 NaGTP, 0.3 Fluo5F, 0.03 AlexaFluor-594, 10 HEPES-KOH (pH 7.4, ~300 mOsm). After filling for 7 min, axons and dendrites were identified in the red channel. Presynaptic boutons were identified by their typical bead-like morphology. Neurons in which the distinction between axons and dendrites was unclear were discarded. Ten minutes after break-in, Ca^{2+} transients were induced by a single action potential evoked via somatic current injection (5 ms, 800–1200 pA). Images were acquired using an Olympus BX51 microscope with a

60×, 1.0 numerical aperture objective. Fluorescence signals were excited by a light-emitting diode at 470 nm and were collected with a scientific complementary metal-oxide-semiconductor camera (ORCA-Flash4.0, Hamamatsu Photonics) at 100 frames/s. In control experiments, no kinetic differences were observed between imaging at 100 Hz or 300 Hz (decay τ at 100 Hz in control neurons, 142 ± 3 ms, $n = 118$ boutons/12 cells/4 batches of cultures; 300 Hz, 140 ± 5 ms, $n = 45/15/4$). Images were collected for 200 ms before and 1 s after the action potential initiation. Neurons were fixed after the experiment using 4% PFA/PBS. The inhibitory neurons were identified using GAD1 antibodies by immunofluorescent staining and confocal microscopy as described above, and the imaged neurons were identified *post hoc* by their Alexa-594 filling. Ca^{2+} transients in inhibitory nerve terminals were quantified using ImageJ. For the analysis in boutons, ROIs were defined using pictures taken in the red channel, and 7–10 boutons were randomly selected from each neuron. After background subtraction (rolling ball with a radius of 1.5 μm), the $(F\text{-}F_0)/F_0$ was calculated (F = average green emission in a bouton at a given time point, F_0 = average fluorescent intensity in frames 0 to 20 before action potential induction). For dendritic measurements, a secondary-order dendrite was selected from each neuron, and the fluorescence from a nearby empty region was referred to as background and subtracted from the ROI. For all Ca^{2+} imaging experiments, the experimenter was blind to the genotype throughout data acquisition and analysis.

Miscellaneous. Southern blotting was performed according to previously published protocols with 32-phosphorus (^{32}P) labeled probes annealing outside of the homology arms of the targeting vector (Rosahl et al., 1993). Electron microscopic analyses were performed on single sections of 2% glutaraldehyde fixed hippocampal neurons as described previously (Kaeser et al., 2011). The number of docked vesicles (defined as vesicles touching the presynaptic plasma membrane), number of vesicles per bouton, postsynaptic density length, and bouton circumference were analyzed in MetaMorph (Molecular Devices) by an experimenter blind to the genotype. Student's *t* test was used to determine statistical significance in all experiments unless stated otherwise.

Results

ELKS proteins are primarily expressed in neurons and localized to synapses

Vertebrate *ELKS* genes are expressed in multiple isoforms. C-terminal splice variants of ELKS1 (ERC1, CAST2) and ELKS2 (ERC2, CAST or CAST1) consist of a predominant presynaptic B-isoform that binds to RIM, or an A-isoform that lacks RIM binding (Wang et al., 2002; Kaeser et al., 2009). ELKS2 also contains alternative promoters that generate a longer α-isoform encoding >95% of the ELKS2 protein, and a shorter β-isoform (Kaeser et al., 2009). Although ELKS was identified as a component of neuronal active zones (Ohtsuka et al., 2002; Wang et al., 2002; Juranek et al., 2006), several studies also support functions for ELKS outside active zones and in non-neuronal cells, for example, a trafficking role via Rab6 (Monier et al., 2002; Grigoriev et al., 2007; Grigoriev et al., 2011) and a role in NF-κB signaling (Ducut Sigala et al., 2004). Given these functions, we reevaluated the hypothesis that ELKS is primarily a neuronal protein. We tested ELKS protein expression in brain and six additional tissues of wild-type mice using multiple antibodies (for isoform specificity of ELKS antibodies used in this study, see Materials and Methods). We found that, in adult mice, ELKS was prominently present in brain, and little ELKS was detectable outside the nervous system, of which the majority was in the lung (Fig. 1*A*). Consistent with previous reports (Wang et al., 2002), this non-neuronal isoform is ELKS1A. We next quantified mRNA levels of ELKS by qRT-PCR (Fig. 1*B*). ELKS2 was largely restricted to the brain, whereas ELKS1 mRNA was high in brain and lung (Fig. 1*B*). To test ELKS localization within the nervous system, we performed immunostainings in cultured hippocampal neurons. ELKS staining was strongly overlapping with the synaptic vesicle marker synapsin. All synapses contained ELKS, and little ELKS was detected outside synapses (Fig. 1*C*). Together, these data confirm that the majority of ELKS is in the brain. Within the nervous tissue, ELKS is largely restricted to synapses.

Knock-out of ELKS1 is lethal

Previous analyses of mammalian ELKS functions in mouse mutants have used conditional or constitutive removal of only ELKS2, abolishing <50% of total ELKS (Kaeser et al., 2009; tom Dieck et al., 2012). We therefore generated conditional ELKS1 KO mice by homologous recombination. In an initial gene targeting approach (see Materials and Methods), we did not obtain surviving homozygote mice for the mutant allele ($ELKS1^{nc}$). We did not restore survival by flp recombination (to remove the neomycin resistance gene, $ELKS1^{nc\text{-}KI}$) or cre recombination (to remove the first coding exon of ELKS1, $ELKS1^{nc\text{-}KO}$). We hypothesized that the genetic manipulation disrupted ELKS1 expression and induced embryonic lethality through loss of ELKS1, and thus all alleles are nonconditional (nc). We adjusted the targeting strategy as described in Materials and Methods and repeated the homologous recombination experiment to generate the $ELKS1^{mutant}$ allele (Fig. 1*D*). Southern blotting confirmed homologous recombination (Fig. 1*E*), and positive clones were used to generate chimeric mice by blastocyst injection. Conditional ($ELKS1^{floxed}$) and constitutive ($ELKS1^{KO}$) ELKS1 KO mice were generated by frt and cre recombination, respectively. Homozygous $ELKS1^{floxed}$ mice expressed ELKS indistinguishable from wild-type littermate controls (Fig. 1*F*); they appeared normal and could be maintained as a homozygous line.

We next evaluated whether the conditional gene targeting is sufficient to remove ELKS1 in cultured hippocampal neurons. Neurons from brains of newborn homozygous $ELKS1^{floxed}$ mice were cultured within 24 h after birth (Maximov et al., 2007; Kaeser et al., 2011) and infected at DIV 5 with lentiviruses expressing a GFP-tagged cre recombinase (to generate cKO neurons) or an inactive mutant of cre (to generate control neurons). Control and cKO neurons are genetically identical, except for the postnatal, cre-mediated removal of ELKS1 (Fig. 1*G*,*H*). This experiment also led to the identification of ELKS1β, which is described below.

We systematically analyzed survival rates in the offspring of heterozygous matings (Fig. 2). Whereas the offspring ratio revealed normal survival of homozygote $ELKS1^{floxed}$ mice, homozygote $ELKS1^{KO}$ mice did not survive to postnatal day 21 (P21; Fig. 2*A*). Mandatory lethality was also observed for the nonconditional lines $ELKS1^{nc\text{-}KI}$ and $ELKS1^{nc\text{-}KO}$ at P21 (Fig. 2*B*) and at embryonic day 14 (E14) and 18 (E18, Fig. 2*C*). These data reveal that removal of ELKS1 leads to embryonic lethality. This phenotype is unlikely due to synaptic functions of ELKS but may be related to other ELKS functions (Monier et al., 2002; Ducut Sigala et al., 2004; Grigoriev et al., 2007; Grigoriev et al., 2011).

Normal presynaptic protein levels in ELKS1/2 conditional double KO neurons

Each vertebrate active zone protein family is typically encoded by multiple genes, and protein functions within the same family are generally redundant (Rosenmund et al., 2002; Schoch et al., 2006; Kaeser et al., 2008, 2011, 2011; Mukherjee et al., 2010). To analyze synaptic functions of ELKS, we circumvented redundancy by crossing $ELKS1^{floxed}$ mice to $ELKS2^{floxed}$ mice (Kaeser et al., 2009). We then generated cultured hippocampal neurons from

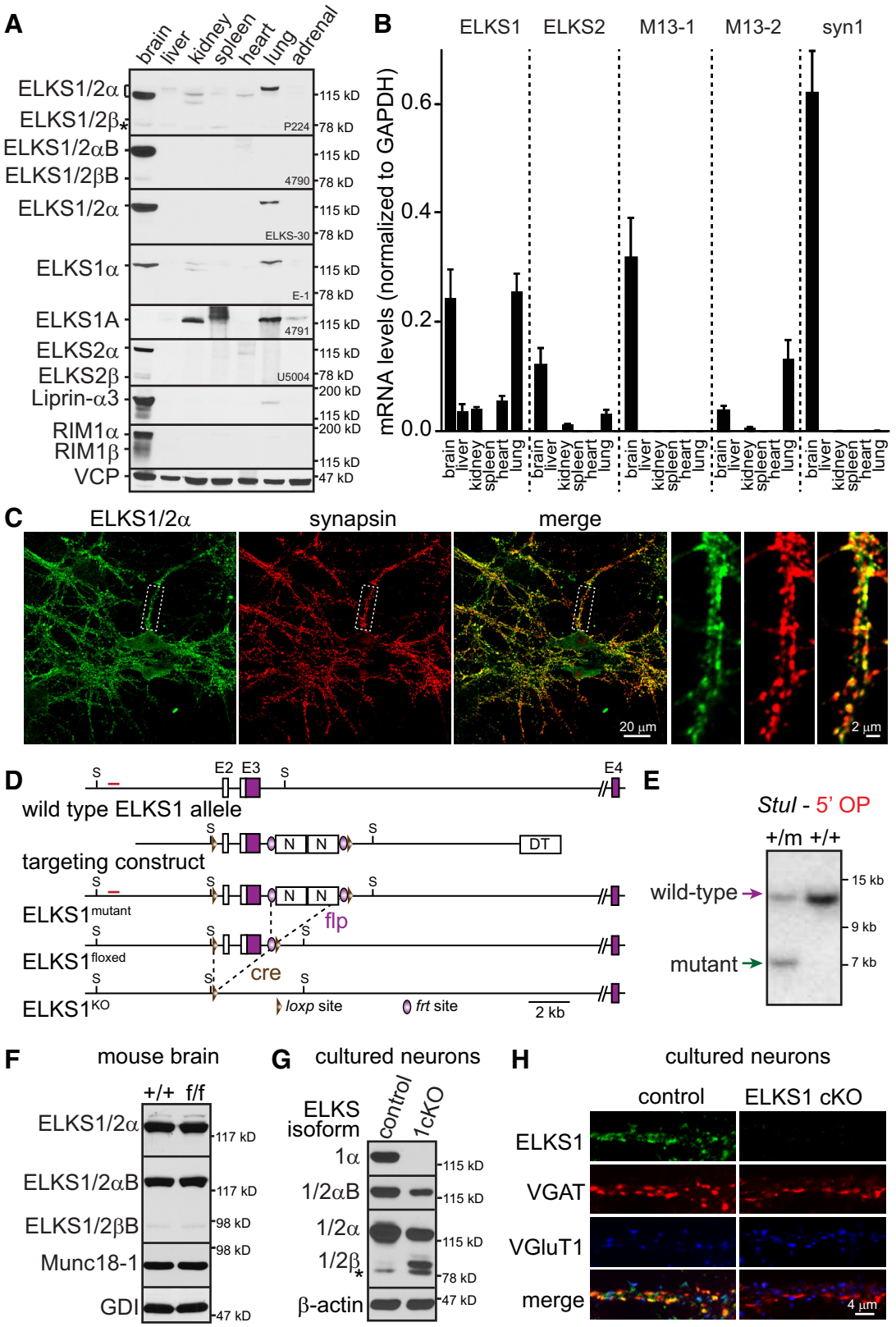

Figure 1. Expression and conditional deletion of ELKS in mice. ***A***, ELKS protein expression in the adult mouse brain and non-neuronal tissues probed with multiple anti-ELKS antibodies (indicated on the bottom right of each panel; for isoform specificity, see Materials and Methods). Molecular weight markers in kilodalton (kDa) are shown on the right. *Nonrelated, cross-reactive band. ***B***, Analysis of mRNA levels (normalized to GAPDH) for ELKS1 and ELKS2 in brain and non-neuronal tissues analyzed by qRT-PCR. The active zone genes Munc13–1 (M13–1) and Munc13–2 (M13–2), and the presynaptic protein synapsin1 (syn1) are used as controls. Each experiment was repeated in three animals; data are normalized to GAPDH and shown as mean ± SEM. ***C***, Immunostaining with antibodies against ELKS (ELKS-30) and synapsin (E028) in cultured hippocampal neurons analyzed by confocal microscopy. ***D***, Revised KO strategy for generating ELKS1 mutant mice. The targeting vector contained a 3′UTR exon and the first coding exon (E2 and E3) flanked by loxp sites, a duplicated neomycin resistance cassette (N) (*Figure legend continues.*)

these mice that lacked both ELKS1 and ELKS2 when infected with cre lentiviruses (ELKS cDKO), or had a complete set of ELKS when infected with a control virus (control). We determined the time course of removal of synaptic ELKS by analyzing the progressive removal of ELKS from synapses after infecting the neurons with synapsin-cre lentiviruses at DIV 5. Markers for synaptic vesicles at inhibitory and excitatory synapses (VGAT and VGluT1, respectively) display punctate staining patterns at DIV 7 (Fig. 3*A*), consistent with the presence of evoked synaptic currents at DIV 7 in cultured hippocampal neurons (Mozhayeva et al., 2002). ELKS immunostaining appeared unaffected at DIV 7 but was visibly reduced starting at DIV 9, and ELKS was entirely absent at DIV 13 (Fig. 3*A*). Thus, we remove ELKS after synapses are established, rendering our manipulation fairly acute relative to synaptogenesis. All functional analyses were done from DIV 14 to DIV 18. Quantitative Western blotting with ^{125}I-labeled antibodies confirmed that cre recombination efficiently removed ELKS protein at DIV 14 without affecting protein levels of other presynaptic proteins (Fig. 3*B*). This suggests that removal of ELKS1 and ELKS2 in cultured hippocampal neurons after DIV 5 does not dramatically affect the development of neurons and synapses *in vitro*.

Unless otherwise noted, cre recombinase expression was driven by a synapsin promoter. The synapsin promoter driven cre lentivirus limited expression of cre in non-neuronal cells (Fig. 3*C*) and was sufficient to remove ELKS (Fig. 3*D*). Its efficiency in removing ELKS was similar to the ubiquitin promoter cre lentivirus that we used in previous studies (Ho et al., 2006; Kaeser et al., 2009, 2011). This supports a neuronal origin of ELKS in these mixed hippocampal cultures.

Comprehensive analysis of ELKS variants expressed in brain

Western blotting also revealed that ELKS1 expressed a shorter variant (Figs. 1*G* and 3*D*), likely via an alternative start codon. Corresponding to a similar protein isoform in the vertebrate ELKS2 gene (Kaeser et al., 2009), we termed this isoform ELKS1β. To determine whether β-ELKS is expressed in wild-type mice, we performed Western blotting on several brain regions throughout postnatal development with an antibody that recognizes α- and β-ELKS (4790, Fig. 4*A*). We found that all brain areas expressed ELKS throughout development, and β-ELKS proteins are detectable at low levels in the striatum, the hippocampus, and the frontal cortex of wild-type mice.

We next assessed β-ELKS expression levels in wild-type and cDKO neurons by quantitative Western blotting using pan-ELKS antibodies (P224) and ^{125}I-coupled secondary antibodies. Together, ELKS1β and ELKS2β account for <5% of total ELKS in wild-type neurons, and in ELKS cDKO neurons β-ELKS is upregulated approximately twofold (Fig. 4*B*). We cloned ELKS1β from mouse neurons by 5′ RACE, and found that it is encoded by an alternative start codon within exon 4 of the *ELKS1* gene (Fig. 4*C*). In the ELKS2 gene, β-ELKS is encoded by an alternative 5′ exon (Kaeser et al., 2009).

These data led to a comprehensive map of ELKS proteins (Fig. 4*D*) with eight principle mammalian ELKS isoforms (ELKS1αA, ELKS1αB, ELKS1βA, ELKS1βB, ELKS2αA, ELKS2αB, ELKS2βA, and ELKS2βB). Of these, α-ELKS isoforms predominate, accounting for >95% of total ELKS, and they are entirely removed in our conditional KO mice. The shorter β-variants are expressed at low levels and are modestly upregulated in the cDKO neurons. It is not known whether β-ELKS localizes to synapses, but our antibodies fail to detect synaptic ELKS in the cDKO neurons.

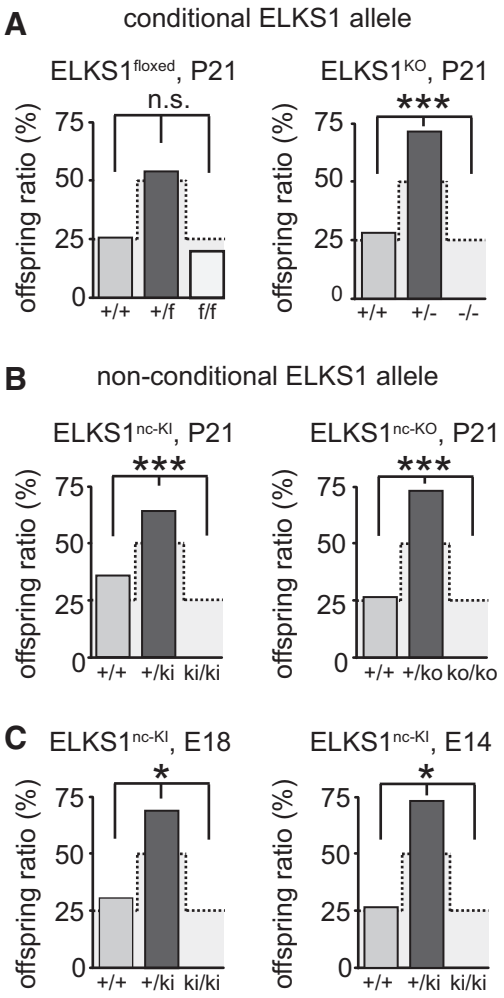

Figure 2. Survival of the ELKS1 alleles. ***A***, Postnatal analysis of survival in heterozygote mating of ELKS1^{floxed} or ELKS1^{KO} mice. A total of 152 mice (ELKS1^{floxed}) or 70 mice (ELKS1^{KO}) were analyzed at postnatal day 21 (P21). Statistical analysis was performed by χ^2 test comparing the expected Mendelian distribution (gray shaded background with dotted line) with the obtained ratio. ***$p < 10^{-5}$ for ELKS1^{KO}. n.s., Not significant. ***B***, A previous attempt with a similar targeting vector (see Experimental methods) resulted in an ELKS1 nonconditional allele (ELKS1^{nc}), and the corresponding flp (ELKS1^{nc-KI}) and cre (ELKS1^{nc-KO}) recombined alleles: analysis of survival in heterozygote mating of the ELKS1^{nc-KI} or ELKS1^{nc-KO} alleles at P21. A total of 183 mice (ELKS1^{nc-KI}) or 64 mice (ELKS1^{nc-KO}) were analyzed. ***$p < 10^{-5}$ (χ^2 test). Zero homozygote ELKS1^{nc-KI} or ELKS1^{nc-KO} mice were obtained. ***C***, Analysis of survival in heterozygote matings of ELKS1^{nc-KI} mice at embryonic day 18 (E18, left) or 14 (E14, right). A total of 23 embryos (E18) or 19 embryos (E14) were analyzed. *$p < 0.05$ (χ^2 test). Zero homozygote ELKS1^{nc-KI} mice were obtained.

←

(*Figure legend continued.*) flanked by frt sites, and a diphtheria toxin (DT) cassette for negative selection. Homologous recombination in ES cells resulted in the conditional ELKS1 mutant allele (ELKS1^{mutant}), and the corresponding flp (ELKS1^{floxed}) and cre (ELKS1^{KO}) recombined alleles. E2-E4, Exons 2–4; S, StuI restriction site. Red bar represents location of the 5′ outside probe used for Southern blotting in ***E***. ***E***, Southern blot using a 5′ outside probe (5′ OP) and StuI digest of genomic DNA from ES cells. Expected band sizes are 12 kb for the wild-type allele and 7 kb band for the targeted allele. ***F***, Representative Western blots of ELKS expression in brain homogenates of an adult wild-type mouse and a homozygous ELKS1^{floxed} littermate mouse. ***G***, ***H***, Expression of ELKS in cultured control and conditional ELKS1 KO neurons (1cKO) as assessed by Western blotting (***G***) and immunostainings imaged on a confocal microscope (***H***). In this and all following figures, KO neurons are neurons of conditional floxed mice infected with lentiviruses expressing cre recombinase and control neurons are identical except for the infection with an inactive mutant of cre. ***G***, *Nonrelated, cross-reactive band.

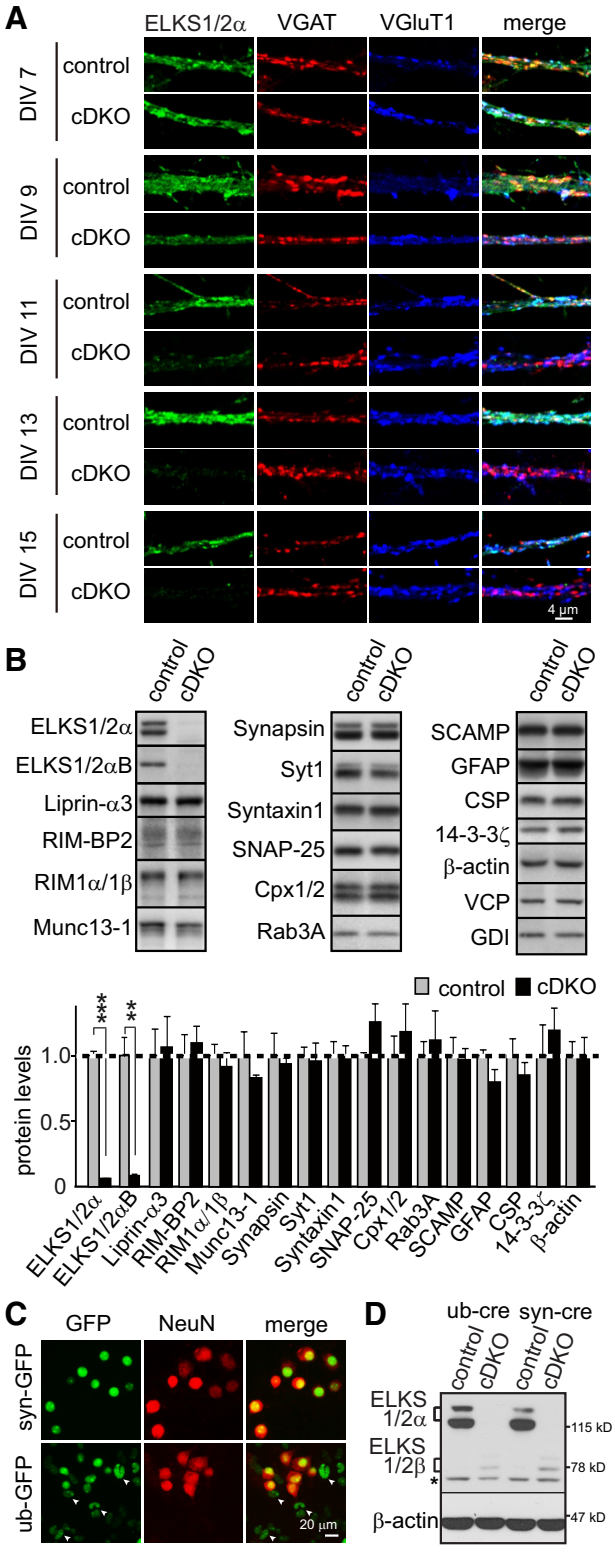

Figure 3. Synaptic protein composition in ELKS cDKO neurons. ***A***, Progressive removal of ELKS as visualized with ELKS-30 antibodies from VGAT- and VGluT1-positive synapses. Neurons were infected with cre and control lentiviruses at DIV 5 and analyzed at intervals of 2 d starting at DIV 7. ***B***, Sample blots (top) and quantitation (bottom) of protein composition of cDKO and control neurons by use of ^{125}I-labeled secondary antibodies. Protein levels are normalized to VCP or GDI. The experiment was repeated in three independent batches of cultures. Data are mean ± SEM. $^{**}p < 0.01$. $^{***}p < 0.001$. Cpx1/2, Complexin 1 and 2; Syt1, Synaptotagmin1. ***C***, Comparison of lentiviral expression of GFP-tagged nuclear cre recombinase (GFP) in mixed hippocampal cultures driven by a human synapsin promoter (top, syn-GFP) or a ubiquitin-promoter (bottom, ub-GFP). NeuN staining is used to identify neurons. White arrowheads indicate nuclei of glial cells that express GFP when driven by a ubiquitin promoter. ***D***, Removal of ELKS1 and ELKS2 protein assessed by Western blotting with pan-ELKS antiserum P224 from cultured neurons of ELKS1^{floxed} × ELKS2^{floxed} mice by infection with lentiviruses expressing cre recombinase under the ubiquitin (left, ub-cre) or synapsin-promoter (right, syn-cre). Control neurons are the same neurons infected with an inactive mutant of cre (control). *Nonrelated, cross-reactive band.

Impaired synaptic transmission at inhibitory synapses in ELKS cDKO neurons

To determine functions of ELKS in neurotransmitter release, we pursued electrophysiological analyses of synaptic transmission in ELKS cDKO and control neurons. We recorded neurons in whole-cell voltage-clamp configuration, using a focal stimulation electrode to stimulate presynaptic neurons. Only cultures in which we detected no noninfected neurons were used, ensuring that presynaptic neurons are devoid of α-ELKS. We focused on characterizing inhibitory synaptic currents because excitatory currents evoke excessive reverberant activity in these cultured neuronal networks, making it more difficult to characterize excitatory synaptic transmission (Maximov et al., 2007; Kaeser et al., 2011). We found that removal of ELKS resulted in an ~50% reduction in synaptic transmission as measured by the amplitude and charge transfer of action potential evoked IPSCs (Fig. 5*A*). In addition, kinetic analyses revealed that the 20%–80% rise time of the IPSC was decreased, and the variability of the rise time across multiple sweeps was increased (Fig. 5*B*). The cDKO and control neurons were indistinguishable in other parameters of the recordings, including IPSC decay kinetics (τ_{fast}: control, 29.6 ± 2.9 ms, $n = 17$ cells/6 batches of cultures; cDKO, 30.5 ± 2.7 ms, $n = 17/6$; τ_{slow}: control, 148.8 ± 14.4 ms, $n = 17/6$; cDKO, 140.0 ± 16.1 ms, $n = 17/6$), membrane resistance (control, 393 ± 41 MΩ, $n = 34/8$; cDKO, 390 ± 58 MΩ, $n = 32/8$), membrane capacitance (control, 106 ± 10 pF, $n = 34/8$; cDKO, 108 ± 9 pF, $n = 32/8$), resting potential (control: −55.6 ± 0.7 mV, $n = 34/8$; cDKO −55.3 ± 0.7 mV, $n = 32/8$; noncompensated), and the number of primary dendrites (control, 4.1 ± 0.2, $n = 34/8$; cDKO, 4.3 ± 0.3, $n = 32/8$). Thus, postnatal deletion of ELKS led to impaired synaptic transmission, but prominent developmental deficits were absent in cultured neurons.

We next asked whether the decrease in synaptic transmission is due to reduced presynaptic neurotransmitter release or whether postsynaptic changes, induced indirectly by deletion of ELKS, might contribute to the reduced IPSC. Removal of ELKS decreased the frequency of mIPSCs by 50% (Fig. 5*C*), which could be due to reduced synapse numbers, or impaired presynaptic release. The mIPSC amplitude was not significantly affected (Fig. 5*C*), nor were the rise and decay kinetics (Fig. 5*D*), suggesting that there is no strong postsynaptic effect of ELKS deletions.

We then measured synaptic transmission in response to paired pulses and analyzed the ratio of the IPSCs ($IPSC_2/IPSC_1$) as a function of the interval between the two pulses. The paired-pulse ratio is typically inversely correlated with release probability p. Inhibitory synapses in cultured hippocampal neurons strongly depressed at short interstimulus intervals, reflecting their high initial p. In the absence of ELKS, the ratio of depression between cDKO and control neurons was impaired by more than a factor of 2 at short intervals (Fig. 5*E*) but was normal when the two stimuli were ≥500 ms apart. These data, together with decreased IPSC amplitudes and decreased mIPSC frequencies, are consistent with a decrease in initial p at inhibitory synapses in ELKS cDKO neurons.

Synaptic morphology in ELKS cDKO neurons

Although constitutive removal of ELKS1 is embryonically lethal, removal of ELKS in neurons did not dramatically alter neuronal membrane properties and synaptic protein composition. However, the decreased IPSC amplitude paralleled by a decreased mIPSC frequency could be in part accounted for by a loss of synapses. We thus quantified the number and size of synaptic puncta labeled with markers for inhibitory and excitatory synapses in ELKS cDKO and control neurons by quantitative confocal microscopy. As quantified on segments of second-order dendrites, the number, size, and intensity of GAD2-positive inhibitory synapses or VGluT1-positive excitatory synapses were unaffected by removal of ELKS (Fig. 6*A*), consistent with the observation that synaptic protein levels were unchanged (Fig. 3*B*). In a second, independent experiment, we measured the number of VGluT1- and VGAT positive terminals in images of randomly selected areas in each coverslip, and the number of inhibitory or excitatory puncta contained in cDKO and control neurons were not changed (data not shown). Electron microscopic analyses of ELKS cDKO synapses in cultured neurons revealed that the synaptic ultrastructure was not noticeably affected in the absence of ELKS (Fig. 6*B*), as none of the parameters we quantified was changed (number of vesicles per bouton: control 68 ± 4, cDKO 76 ± 4; number of docked vesicles per active zone: control 2.7 ± 0.2, cDKO 2.6 ± 0.2; number of vesicles within 150 nm of the active zone: control 10.2 ± 0.6, cDKO 8.9 ± 0.5; post synaptic density length: control 437 ± 22 nm, cDKO 485 ± 24 nm; bouton circumference: control 3.3 ± 0.1 μm, cDKO 3.3 ± 0.1 μm; synapse density (synapses per 12.5 μm^2): control 3.0 ± 0.2, cDKO 3.1 ± 0.2). These experiments suggest that postnatal ELKS removal does not lead to dramatic effects in synapse density or ultrastructure in cultured hippocampal neurons and support that conditional removal of ELKS1 and ELKS2 impairs neurotransmitter release at inhibitory nerve terminals. Such a defect could either be due to impaired Ca^{2+} triggering of release or a decrease in the RRP.

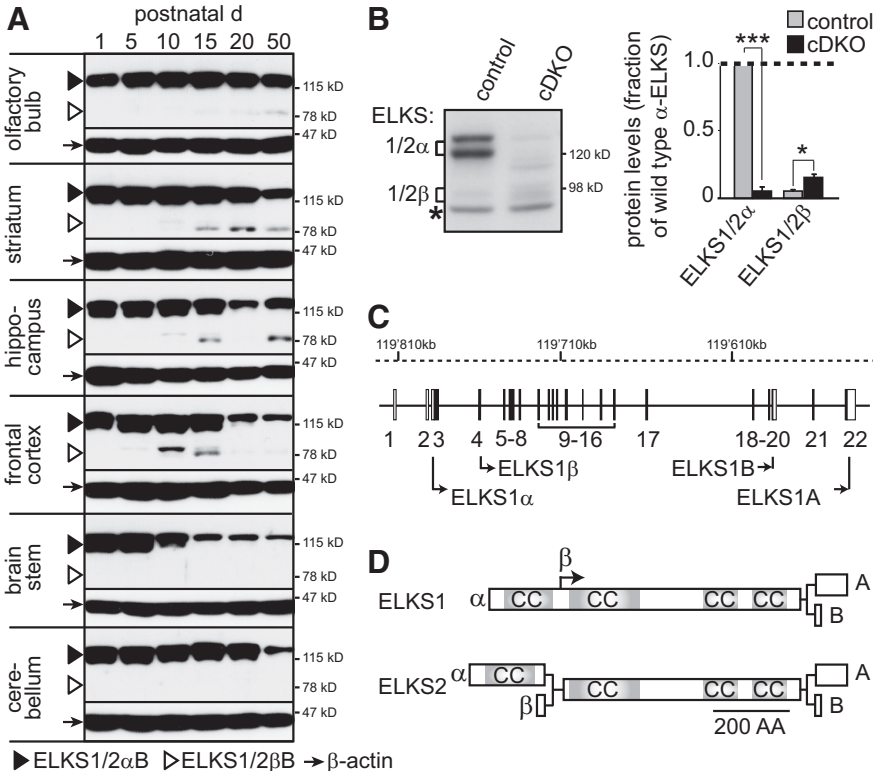

Figure 4. Identification of ELKS1β. ***A***, Expression profile of ELKS proteins from postnatal day 1 to 50 in six different brain areas with an antibody that recognizes all C-terminal B splice variants of ELKS (4790, see Materials and Methods), including ELKS1β and ELKS2β isoforms. For each brain area, a blot for β-actin is shown as a loading control. ***B***, Sample blot and quantitation of levels of ELKS1/2β expression in control and ELKS cDKO neurons. Western blots were preformed with pan-ELKS antiserum P224 as a primary antibody and with ^{125}I-labeled secondary antibodies, and ELKS1/2β was normalized to wild-type ELKS1/2α. *Nonrelated, cross-reactive band. ***C***, Map of the murine *ELKS1* gene. The *ELKS1* gene produces N-terminal promoter variants termed α and β, and C-terminal splice variants B (contains a C-terminal PDZ domain binding motif) and A. ELKS1β is expressed from an alternative start codon within exon 4, as identified by 5′ RACE analysis. ***D***, Map of ELKS proteins. A total of eight ELKS proteins are expressed in mammals: ELKS1αB, ELKS1αA, ELKS1βB, ELKS1βA, ELKS2αB, ELKS2αA, ELKS2βB, and ELKS2βA.

Impaired Ca^{2+} triggering of release in ELKS cDKO neurons

The observation that paired-pulse depression was impaired and the rise time increased led to the hypothesis that ELKS may be required for normal Ca^{2+} triggering of release at inhibitory synapses. To evaluate Ca^{2+} triggering of release in cDKO neurons, we characterized the dependence of release on the extracellular Ca^{2+} concentration ($[Ca^{2+}]_{ex}$) (Dodge and Rahamimoff, 1967). At high $[Ca^{2+}]_{ex}$, Ca^{2+} triggering of release saturates, Ca^{2+} flux through Ca^{2+} channels may also saturate, and postsynaptic receptors may saturate or desensitize, leading to a saturated measurement of synaptic transmission. Although this experiment does not directly reveal the mechanism of Ca^{2+} triggering, it has proven useful to identify defects in Ca^{2+} sensing or Ca^{2+} influx in gene mutants (Fernández-Chacón et al., 2001; Sorensen et al., 2003; Sun et al., 2007; Kaeser et al., 2011). In ELKS cDKO neurons, IPSC amplitudes were decreased at all $[Ca^{2+}]_{ex}$ (Fig. 7*A*), and the $[Ca^{2+}]_{ex}$ dependence was right-shifted when normalized to the largest response (Fig. 7*B*). Fitting each experiment to a Hill function revealed that Ca^{2+} cooperativity of release was unchanged, but that the effective $[Ca^{2+}]_{ex}$ at which we observed the half-maximal IPSC (EC_{50} of $[Ca^{2+}]_{ex}$, sometimes referred to as Ca^{2+} affinity) was significantly increased (Fig. 7*C*). These data are consistent with impaired Ca^{2+} triggering of release and suggest that low $[Ca^{2+}]_{ex}$ enhances the impairment in release observed in ELKS cDKO neurons.

We hypothesized that impaired Ca^{2+} triggering in ELKS cDKO neurons also led to the slowed release observed in Figure 5*B*. If this hypothesis is correct, increasing $[Ca^{2+}]_{ex}$ should accelerate release in ELKS cDKO neurons, and decreasing $[Ca^{2+}]_{ex}$ should slow down release in wild-type neurons. When we determined the dependence of the rise times on $[Ca^{2+}]_{ex}$, we found that this is the case (Fig. 7*D*). We next examined whether the mIPSC frequencies are decreased in ELKS cDKO mutants at low $[Ca^{2+}]_{ex}$. Compellingly, mIPSC frequencies were similar in 0.5 mM $[Ca^{2+}]_{ex}$ between cDKO and control neurons and identical in 0 mM $[Ca^{2+}]_{ex}$/1 mM EGTA. This experiment also revealed that there was no genotype effect on mIPSC rise kinetics at various $[Ca^{2+}]_{ex}$ (20%–80% rise time: 2 mM $[Ca^{2+}]_{ex}$ as shown in Fig. 5*D* control; 0.5 mM $[Ca^{2+}]_{ex}$ control, 1.37 ± 0.07 ms, $n = 21$

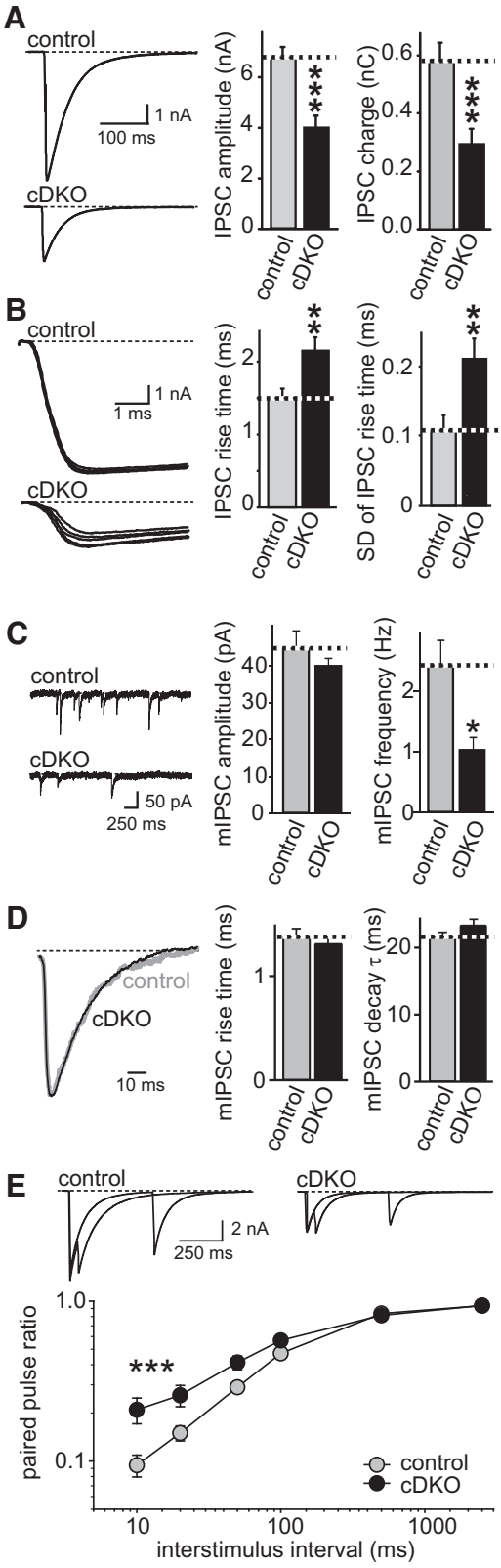

Figure 5. Impaired inhibitory synaptic transmission in ELKS-deficient neurons. ***A***, Sample traces (left) and quantitation (right) of evoked IPSCs in ELKS cDKO and control neurons (control $n = 28$ cells/4 independent batches of cultures, cDKO $n = 27/4$). ***B***, Analysis of the 20%–80% rise time and the SD of the 20%–80% rise time of IPSCs in control and cDKO neurons (control $n = 30/5$, cDKO $n = 28/5$). ***C***, Analysis of mIPSC amplitude and frequency in control and cDKO neurons (control $n = 12/3$, cDKO $n = 13/3$). ***D***, Analysis of mIPSC 20%–80% rise time and decay τ in control and cDKO neurons (control $n = 16$ cells/3 batches of cultures, cDKO $n = 16/3$). ***A–D***, Data are mean ± SEM. $^*p < 0.05$. $^{**}p < 0.01$. $^{***}p < 0.001$. ***E***, Sample trace (top) and summary graph (bottom) of paired pulse ratios of IPSCs in ELKS cDKO and control neurons plotted as a function of the interstimulus interval (control $n = 15/4$, cDKO $n = 13/4$). Data are mean ± SEM. Significance was analyzed by two-way ANOVA: genotype, $^{***}p < 0.0001$; $[Ca^{2+}]_{ex}$, $^{***}p < 0.0001$; interaction, $^*p < 0.05$. Tukey post test: $^*p < 0.05$ at 50 ms.

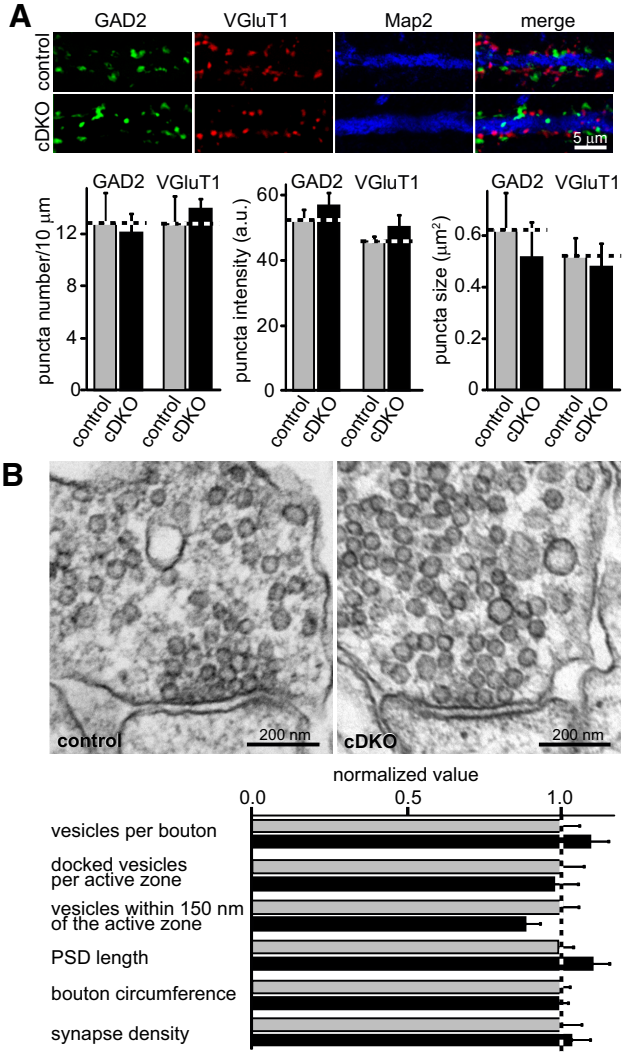

Figure 6. Normal synapse density and synaptic morphology in the absence of ELKS. ***A***, Sample image of stainings for GAD2-positive inhibitory and VGluT1-positive excitatory synapses (top) and quantitation (bottom) of the number, intensity, and size of these synapses in ELKS cDKO and control neurons (control $n = 3$ cultures, cDKO $n = 3$). ***B***, Sample images and quantitative analyses of electron microscopic images of ELKS cDKO and control synapses (control $n = 40$ synapses, cDKO $n = 43$). Absolute values are provided in the text. Data are mean ± SEM. No significant differences were observed.

cells/3 batches of cultures; 0.5 mM $[Ca^{2+}]_{ex}$ cDKO, 1.44 ± 0.07 ms, $n = 20/3$; 0 mM $[Ca^{2+}]_{ex}$ control, 1.37 ± 0.07 ms, $n = 25/3$; 0 mM $[Ca^{2+}]_{ex}$ cDKO, 1.44 ± 0.06 ms, $n = 28/3$) and decay kinetics (decay τ: 2 mM $[Ca^{2+}]_{ex}$ as shown in Fig. 5*D*; 0.5 mM $[Ca^{2+}]_{ex}$ control, 22.4 ± 0.83 ms, $n = 21/3$; 0.5 mM $[Ca^{2+}]_{ex}$ cDKO, 22.2 ± 0.85 ms, $n = 20/3$; 0 mM $[Ca^{2+}]_{ex}$ control, 23.4 ± 0.76 ms, $n = 25/3$; 0 mM $[Ca^{2+}]_{ex}$ cDKO, 25.4 ± 0.72 ms, $n = 28/3$). As already illustrated in Figure 5*C*, there was a trend toward a very small reduction in mIPSC amplitudes at all $[Ca^{2+}]_{ex}$. This trend became significant when we analyzed the experiment shown in Figure 7*E* by two-way ANOVA (2 mM $[Ca^{2+}]_{ex}$: con-

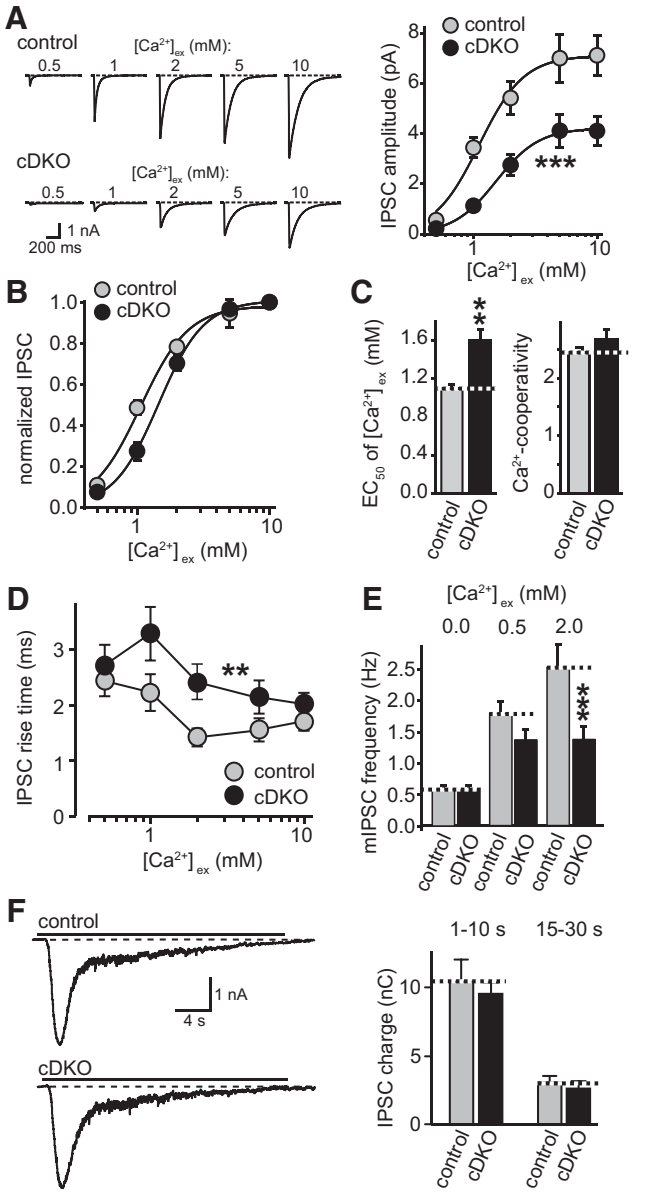

Figure 7. Impaired Ca^{2+} triggering of release in ELKS cDKO synapses. ***A***, Representative traces (top) and summary graph of the Ca^{2+} dependence of IPSCs in ELKS cDKO and control neurons. IPSC amplitudes are plotted as absolute values. Significance was analyzed by two-way ANOVA: genotype, $***p < 0.005$; $[Ca^{2+}]_{ex}$, $***p < 0.005$; interaction, not significant. ***B***, IPSC amplitudes plotted normalized to the response recorded at 10 mM $[Ca^{2+}]_{ex}$. ***C***, EC_{50} of $[Ca^{2+}]_{ex}$ and Ca^{2+} cooperativity as determined by fitting each experiment to a Hill function. $**p < 0.01$. ***D***, IPSC rise time as a function of $[Ca^{2+}]_{ex}$ in control and ELKS cDKO neurons. Significance was analyzed by two-way ANOVA: genotype, $**p < 0.01$; $[Ca^{2+}]_{ex}$, $**p < 0.01$; interaction, not significant. ***A–D***, Control $n = 9$ neurons/3 independent cultures, cDKO $n = 12/3$). ***E***, mIPSC frequency as a function of $[Ca^{2+}]_{ex}$ in control and ELKS cDKO neurons. The 0 mM $[Ca^{2+}]_{ex}$ recordings were obtained in extracellular solution containing 1 mM EGTA. Significance was analyzed by two-way ANOVA: genotype, $***p < 0.005$; $[Ca^{2+}]_{ex}$, $***p < 0.005$; interaction, $***p < 0.005$. Tukey post test: $***p < 0.005$ at 2 mM $[Ca^{2+}]_{ex}$, no significant differences at 0 and 0.5 mM $[Ca^{2+}]_{ex}$. The 0 mM $[Ca^{2+}]_{ex}$ control, $n = 25$ cells/3 batches of cultures; cDKO, $n = 28/3$. The 0.5 mM $[Ca^{2+}]_{ex}$ control, $n = 21/3$; cDKO, $n = 20/3$. The 2 mM $[Ca^{2+}]_{ex}$ control, $n = 16/3$; cDKO, $n = 16/3$). ***F***, Sample trace (left) and summary graph (right) of the RRP as measured by application of hypertonic sucrose for 30 s (black line on top of sample trace) to cDKO and control neurons (control $n = 8/3$, cDKO $n = 10/3$).

trol, 45.0 ± 2.4 pA, $n = 16$ cells/3 independent cultures; cDKO, 39.0 ± 2.4 pA, $n = 16/3$; 0.5 mM $[Ca^{2+}]_{ex}$: control, 40.6 ± 2.1 pA, $n = 21/3$; cDKO, 33.1 ± 2.2 pA, $n = 20/3$; 0 mM $[Ca^{2+}]_{ex}$: control, 41.0 ± 1.9 pA, $n = 25/3$; cDKO, 33.6 ± 1.8 pA, $n = 28/3$; genotype: $p < 0.0001$, $[Ca^{2+}]_{ex}$: not significant, interaction: not significant). The origin of this effect is currently not known. Together, our data reveal that the Ca^{2+} dependence of action potential triggered and spontaneous release is significantly impaired in ELKS cDKO neurons.

In a subsequent experiment, we monitored release by measuring the IPSC induced by focal application of 0.5 M sucrose, a method that releases the entire RRP independent of Ca^{2+} triggering (Rosenmund and Stevens, 1996). This Ca^{2+}-independent form of release was not affected in the cDKO neurons (Fig. 7*F*), which was surprising because we previously showed that ELKS2α suppresses RRP (Kaeser et al., 2009). Our data are consistent with the hypothesis that ELKS1 and ELKS2 may have opposing regulatory effects on the RRP, which could be offset in the absence of both proteins.

In summary, the synaptic deficits described thus far are reminiscent of a defect in Ca^{2+} triggering of release, supporting that removal of ELKS leads to a reduction in release probability p at physiological $[Ca^{2+}]_{ex}$. This deficit could reflect either changes in Ca^{2+} influx or changes in the intracellular Ca^{2+} dependence of release, such as Ca^{2+} buffering, Ca^{2+} sensing, or the spatial coupling of Ca^{2+} influx and Ca^{2+} sensing. We next sought to distinguish between these possibilities.

ELKS enhances Ca^{2+} influx at inhibitory nerve terminals

To test whether Ca^{2+} influx is impaired in ELKS cDKO synapses, we performed measurements of presynaptic Ca^{2+} influx induced by single action potentials selectively in inhibitory nerve terminals (Fig. 8). Presynaptic neurons were patched and filled with fixable AlexaFluor 594 and the Ca^{2+}-indicator Fluo5F through the patch pipette for 10 min. The axon and presynaptic boutons were identified in the red channel. A brief somatic current injection through the patch pipette was used to induce a single action potential, and Ca^{2+} influx was monitored in the green channel at individual presynaptic nerve terminals and in the dendritic arbor with a scientific complementary metal-oxide-semiconductor camera. Single action potential-induced Ca^{2+} influx was quantified as the $\Delta F/F_0$, where F_0 reflects baseline Fluo5F fluorescence before the action potential in an individual bouton or dendrite, and ΔF is the Fluo5F fluorescence at any time during the imaging minus F_0. In this experiment, the measured Ca^{2+} transients are triggered by the action potential because no transients are observed when the neurons are stimulated in the presence of TTX to block action potentials (without TTX $\Delta F/F_0 = 4.76 \pm 0.52$, $n = 30$ boutons/3 cells; with TTX $\Delta F/F_0 = 0.045 \pm 0.004$, $n = 30/3$), or when a subthreshold current injection is used (Kaeser et al., 2011). After imaging, neurons were fixed and immunostained with antibodies against GAD1, a somatic marker for inhibitory neurons (Kaufman et al., 1991; Lau and Murthy, 2012), and we identified the recorded neuron by its filling with AlexaFluor 594. This approach allowed analyzing Ca^{2+} influx exclusively in inhibitory neurons, and GAD1-negative neurons were not included in the analysis (Fig. 8*C*). Compellingly, ELKS cDKO revealed an ~30% decrease in peak presynaptic Ca^{2+} influx in inhibitory nerve terminals (Fig. 8*D*), but dendritic Ca^{2+} influx remained unaltered (Fig. 8*D*, inset). We conclude that ELKS boosts presynaptic Ca^{2+} influx at inhibitory nerve terminals. This conclusion also strongly supports the hypothesis that ELKS enhances initial release probability at these synapses.

It is possible that some of the changes we observe are due to a change in the waveform of the action potential. Thus, we determined whether removal of ELKS changes the somatic action potential in the neurons used for the analysis of Ca^{2+} influx. ELKS

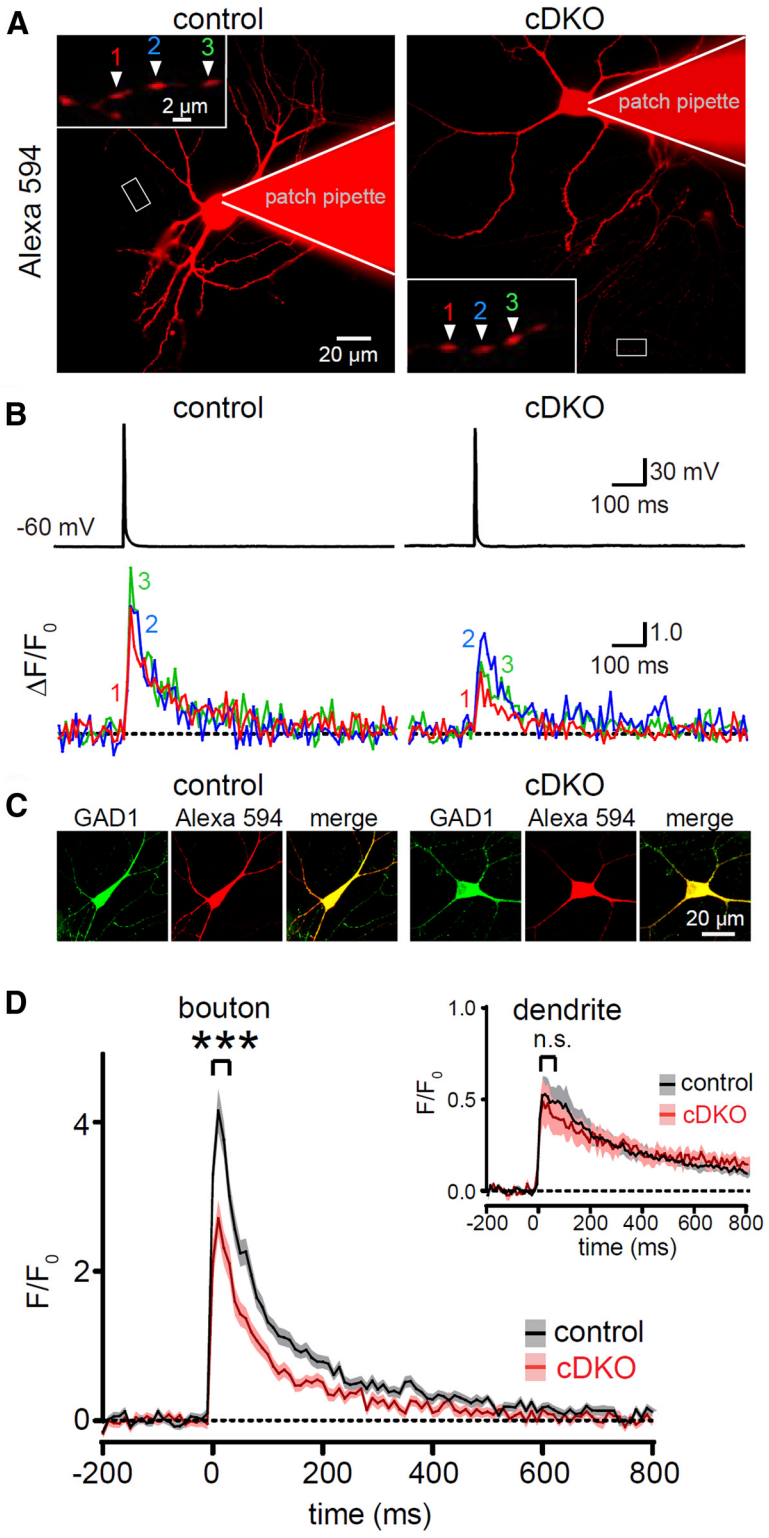

Figure 8. Impaired Ca^{2+} influx at inhibitory nerve terminals in ELKS cDKO neurons. ***A***, Representative images of control and cDKO neurons filled via a patch pipette with Fluo5F and AlexaFluor 594 (red, shown). Insets, Enlarged view of boutons analyzed in ***B***. ***B***, Somatic action potentials (top) and quantifications of the presynaptic Ca^{2+} transients imaged via Fluo5F fluorescence (bottom) of the boutons shown in ***A***. ***C***, *Post hoc* immunostainings with GAD1 antibodies (green) of the recorded neurons identified by their filling with AlexaFluor 594. ***D***, Summary plots of single action potential-induced Ca^{2+} transients in presynaptic boutons from control and cDKO inhibitory neurons. Inset, Same plot for dendrites. Data are shown as mean (line) ± SEM (shaded area). $^{***}p < 0.001$ for peak amplitudes during the first 60 ms after the action potential as assessed by two-way ANOVA for genotype and time, not significant for interaction (control $n = 92$ boutons/11 cells/4 independent cultures, cDKO $n = 64/7/4$; control $n = 11$ dendrites/11 cells/4 independent cultures, cDKO $n = 7/7/4$).

cDKO neurons were indistinguishable from control neurons in the half-width (control, 1.74 ± 0.13 ms, $n = 11$ cells/4 batches of cultures; cDKO, 1.76 ± 0.1 ms, $n = 7/4$), the maximal rise slope (control, 118 ± 11 V/s, $n = 11/4$; cDKO, 98 ± 12 V/s, $n = 7/4$), the maximal decay slope (control, 51 ± 3.6 V/s, $n = 11/4$; cDKO, 49 ± 3.5 V/s, $n = 7/4$), and the ratio between rise and decay (control, 2.1 ± 0.3, $n = 11/4$; cDKO, 2.3 ± 0.2, $n = 7/4$). To further probe for effects of ELKS deletions on Na^+ currents, we pursued additional current-clamp experiments in the presence of TEA to block voltage-gated K^+ channels. Again, removal of ELKS did not affect the half-width (control, 3.91 ± 0.26 ms, $n = 26$ cells/3 batches of cultures; cDKO, 4.48 ± 0.37 ms, $n = 28/3$), the amplitude (control, 84.3 ± 2.2 mV, $n = 26/3$; cDKO, 82.8 ± 2.2 mV, $n = 28/3$), the maximal rise slope (control, 159.5 ± 9.5 V/s, $n = 26/3$; cDKO, 142.8 ± 8.6 V/s, $n = 28/3$) and the maximal decay slope (control, 26.1 ± 1.92 V/s, $n = 26/3$; cDKO, 23.3 ± 2.4 V/s, $n = 28/3$) of the somatic action potential. Although we cannot exclude changes in the waveform in the presynaptic nerve terminal, these data demonstrate that ELKS removal does not affect the somatic action potential. The observation that mIPSC frequencies are only affected in 2 mM $[Ca^{2+}]_{ex}$ but normal when $[Ca^{2+}]_{ex}$ is removed (Fig. 7*E*) further supports that the $[Ca^{2+}]_{ex}$ dependence of release is affected in ELKS cDKO neurons independent of the action potential waveform.

In summary, these experiments reveal a 30% decrease in presynaptic Ca^{2+} influx in inhibitory nerve terminals of ELKS cDKO neurons.

Localization and expression of presynaptic Ca^{2+} channels in ELKS cDKO neurons

Other active zone proteins, such as RIMs and RIM-BPs, enhance presynaptic Ca^{2+} influx (Han et al., 2011; Kaeser et al., 2011; Liu et al., 2011). It was found that these proteins operate by physical tethering of presynaptic Ca^{2+} channels to release sites (Hibino et al., 2002; Kaeser et al., 2011; Liu et al., 2011), a function that is also shared with bassoon and brp (Kittel et al., 2006; Frank et al., 2010; Davydova et al., 2014). Thus, to date, genetic removal of active zone proteins suggests that these proteins physically tether Ca^{2+} channels to release sites. Consequently, we hypothesized that ELKS may contribute to the localization of presynaptic Ca^{2+} channels and that, in the absence of ELKS, their lo-

calization and/or their expression levels may change. We thus set out to test whether the localization or expression of presynaptic Ca^{2+} channels is impaired in ELKS cDKO neurons. Several presynaptic Ca^{2+} channels contribute to neurotransmitter release. The main pore-forming α-subunits that trigger release in hippocampal neurons are $Ca_V2.1$ and $Ca_V2.2$ channels, and the main auxiliary β-subunits in brain are $Ca_V\beta3$ and $Ca_V\beta4$ (Dolphin, 2003; Cao et al., 2004; Catterall et al., 2005; Kaeser et al., 2011). Thus, we focused on these α- and β-subunits. Quantitative confocal analyses of immunofluorescent stainings revealed that the synaptic levels of the $Ca_V2.1$, $Ca_V2.2$, and $Ca_V\beta3$ subunits are indistinguishable as quantified at inhibitory synapses of ELKS cDKO and control neurons (Fig. 9*A*). Importantly, similar experiments were sufficient to detect a defect in $Ca_V2.1$ Ca^{2+} channel localization in synapses void of RIM (Kaeser et al., 2011) or bassoon (Davydova et al., 2014). Similarly, the protein levels as quantified by Western blotting using fluorescent secondary antibodies (Fig. 9*B*) and the mRNA levels measured by qRT-PCR (Fig. 9*C*) were unchanged. Although we cannot exclude mild effects on the tethering of presynaptic Ca^{2+} channels in cDKO neurons, these data suggest that ELKS removal has no major effect on levels or localization of presynaptic Ca^{2+} channels. This raises the possibility that ELKS operates via a mechanism different from controlling the levels of presynaptic Ca^{2+} channels.

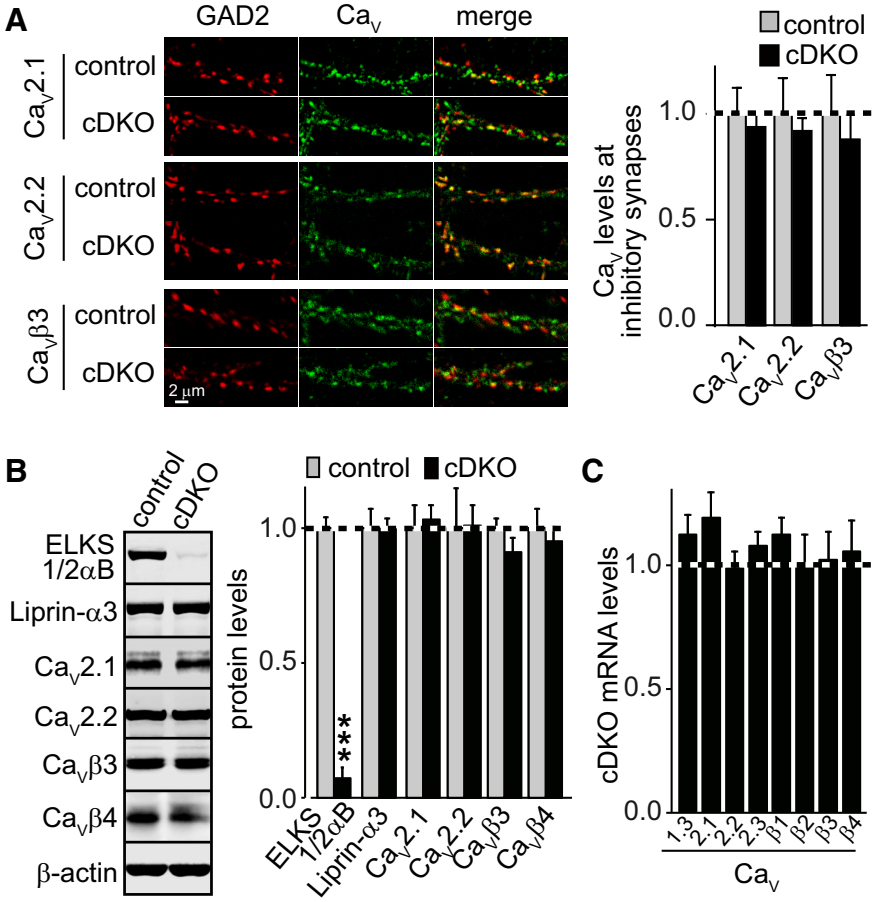

Figure 9. Normal expression and localization of presynaptic Ca^{2+} channels in ELKS cDKO neurons. ***A***, Sample images (left) and quantitative analyses (right) of immunofluorescent stainings of $Ca_V2.1$, $Ca_V2.2$, and $Ca_V\beta3$ Ca^{2+} channel subunits at GAD2-positive inhibitory nerve terminals ($Ca_V2.1$: control $n = 6$ independent cultures, cDKO $n = 6$; $Ca_V2.2$ and $Ca_V\beta3$: control $n = 5$, cDKO $n = 5$). ***B***, Sample blots (left) and quantitation (right) of $Ca_V2.1$, $Ca_V2.2$, $Ca_V\beta3$, and $Ca_V\beta4$ protein levels in cDKO and control neurons by use of fluorescently tagged secondary antibodies. Protein levels are normalized within each sample to β-actin and expressed relative to control. The experiment was repeated in three independent batches of cultures; data are mean ± SEM. ***$p < 0.001$. ***C***, mRNA levels of the presynaptic $Ca_V2.1$, $Ca_V2.2$, and $Ca_V2.3$ Ca^{2+} channel α-subunits, all four β-subunits, and $Ca_V1.3$ subunits as controls in cDKO and control neurons. mRNA levels are normalized to synapsin1 within each sample and expressed relative to control. The experiment was repeated in three independent batches of cultures; data are mean ± SEM. No significant differences were observed.

Discussion

We here used a systematic genetic approach to determine synaptic functions of ELKS, a family of proteins predominantly localized to presynaptic active zones (Fig. 1) (Ohtsuka et al., 2002; Wang et al., 2002). Using newly generated KO mice for ELKS1, we found that ELKS1 removal leads to embryonic lethality (Fig. 2). To circumvent lethality and compensatory effects through redundant functions of ELKS1 and ELSK2, we used conditional removal of ELKS1 and ELKS2 in cultured hippocampal neurons after synapses are established (Fig. 3). We find that ELKS enhances presynaptic Ca^{2+} influx to boost p at inhibitory hippocampal nerve terminals (Figs. 5, 6, 7, and 8). Unlike the vertebrate active zone proteins RIM and RIM-BP (Kaeser et al., 2011), ELKS may not operate by tethering of Ca^{2+} channels to the active zone (Fig. 9). Our results support the hypothesis that vertebrate active zone proteins not only localize channels to release sites but may be important for modulation of Ca^{2+} channel function.

Controlling presynaptic Ca^{2+} by active zone proteins

Previous studies have shown that active zone proteins tether Ca^{2+} channels to release sites. A well-understood tethering mechanism operates by a tripartite complex between RIM, RIM-BP, and Ca_V2 channels (Hibino et al., 2002; Kaeser et al., 2011). These interactions localize Ca^{2+} channels to release sites for fast Ca^{2+} triggering of synaptic vesicle exocytosis (Han et al., 2011; Kaeser et al., 2011). These findings are supported by recent observations at the *Drosophila* NMJ, where RIM is required for normal Ca^{2+} influx (Müller et al., 2012), and RIM-BP promotes Ca^{2+} influx and tethers tagged Ca^{2+} channels (Liu et al., 2011). In addition, bassoon was shown to organize Ca^{2+} channels at a ribbon-containing active zone (Frank et al., 2010), and to be involved in tethering $Ca_V2.1$ channels to active zones via RIM-BP (Davydova et al., 2014). Brp furthermore enhances localization of tagged Ca^{2+} channels at the *Drosophila* NMJ (Kittel et al., 2006). Thus, disturbing active zone architecture by removing RIMs, RIM-BPs, brp, or bassoon leads to decreased Ca^{2+} channel tethering. To our knowledge, removal of ELKS is the first genetic manipulation of an active zone protein that impairs presynaptic Ca^{2+} influx but does not dramatically reduce presynaptic localization of the Ca^{2+} channels. These observations are consistent with the hypothesis that ELKS modulates channel opening. Modulation of Ca^{2+} channel opening by active zone proteins has been

proposed based on studies in non-neuronal cells. In these experiments, cotransfection of Ca^{2+} channels and RIMs (Kiyonaka et al., 2007; Kaeser et al., 2012), ELKS (Kiyonaka et al., 2012) or bassoon (Nishimune et al., 2012) led to changes in depolarization-induced Ca^{2+}-currents in non-neuronal cells. However, these *in vitro* observations have not been validated in nerve terminals. RIM, for example, shifts Ca^{2+} channel inactivation to higher voltage (Kiyonaka et al., 2007; Kaeser et al., 2012), but genetic experiments in neurons did not support a synaptic function of this *in vitro* effect (Han et al., 2011; Kaeser et al., 2012). ELKS was recently shown to bind to β-subunits of Ca^{2+} channels (Billings et al., 2012; Kiyonaka et al., 2012), and one study suggested that ELKS2 shifts Ca^{2+} channel activation to more hyperpolarized potentials in transfected, non-neuronal cells (Kiyonaka et al., 2012). Our data are consistent with such an effect in neurons if it is assumed that ELKS1 and ELKS2 are redundant in this function. Redundancy is supported biochemically because ELKS1 and ELKS2 bind to $Ca_V\beta 4$ subunits of Ca^{2+} channels (Billings et al., 2012; Kiyonaka et al., 2012). The notion that our genetic manipulation removes ELKS after synaptogenesis further supports an acute role for ELKS in enhancing Ca^{2+} influx. However, our findings are also consistent with other hypotheses, for example, that ELKS directly modulates pore-forming α-subunits, that it recruits an unknown protein to modulate Ca^{2+} channel function, or that ELKS cDKO leads to retention of Ca^{2+} channels within nerve terminals. Future studies will be required to determine the molecular mechanisms by which ELKS boosts Ca^{2+} influx.

Brp is a partial ELKS homolog in *Drosophila* (Monier et al., 2002; Wagh et al., 2006), and it supports clustering of tagged Ca^{2+} channels at the larval NMJ (Kittel et al., 2006). The mechanism for Ca^{2+} channel tethering by brp is not completely understood, and it has not been determined whether brp is necessary for normal Ca^{2+} influx. Our results suggest that there is functional redundancy between brp and vertebrate ELKS because both proteins enhance *p*. However, their mechanisms are likely different. Whereas brp is necessary for tethering of Ca^{2+} channels, at least when they are overexpressed, ELKS does not appear to be necessary for localizing Ca^{2+} channels to nerve terminals.

Roles for ELKS in determining RRP

Our data show that, in inhibitory ELKS cDKO neurons, the RRP as defined by exocytosis induced by hypertonic sucrose is unchanged. Nevertheless, it is well established that ELKS has roles in determining RRP size. The first evidence for a function of ELKS in determining the RRP was found at inhibitory synapses of ELKS2α KO mice, where ELKS2α suppressed the RRP (Kaeser et al., 2009). These data, together with our current observation, are consistent with the hypothesis that ELKS has both isoform and synapse-specific roles in determining RRP, perhaps through intricate interplay between ELKS isoforms. Isoform-specific roles in RRP are supported by experiments in brp-deficient flies. Brp has a genetic organization reminiscent of vertebrate α- and β-ELKS, generating two N-terminally distinct brp proteins (Matkovic et al., 2013). The complete brp null mutant has a normal RRP size (Hallermann et al., 2010a), but a recent study found that, if individual variants of brp were removed, relatively mild effects on RRP size were uncovered (Matkovic et al., 2013). Thus, complete removal of ELKS or brp does not lead to an effect on the inhibitory RRP or the RRP at the fly NMJ, respectively, but deletion of individual genes in vertebrates or individual isoforms in *Drosophila* leads to changes in RRP size. What could the mechanisms that underlie these observations be?

For vertebrate ELKS, the most parsimonious model is that ELKS1 and ELKS2 modulate the RRP in opposite directions, perhaps in a competitive manner. Several pieces of data support such a hypothetical model. First, ELKS2α suppresses the RRP in a subset of synapses in the hippocampus (Kaeser et al., 2009). Second, this pool deficit is offset in the absence of ELKS1 and ELKS2 (Fig. 8). Given their sequence similarity, it is possible that ELKS1 and ELKS2 compete for localization at the active zone. The observation that constitutive deletion of ELKS2/CAST enhances levels of ELKS1 in the retina (tom Dieck et al., 2012) is consistent with such a competitive relationship between ELKS1 and ELKS2. Thus, it is possible that interplay between ELKS1 and ELKS2 regulates the RRP, a hypothesis that could explain why ELKS2α KO synapses have an increased RRP.

Finally, RRP measurements in ELKS2 KO (Kaeser et al., 2009) and ELKS cDKO (current study) neurons define the RRP as vesicles released in response to hypertonic sucrose. Although this RRP largely overlaps with the RRP used by action potentials (Rosenmund and Stevens, 1996), it is possible that ELKS has functions in RRP that are not uncovered by sucrose application. The observation that increasing extracellular Ca^{2+} only partially rescues the IPSC amplitude (Fig. 7) is consistent with such a function. Studies at specific synapses using RRP measurements by action potentials, which is not possible in our cultured neurons because of receptor saturation and desensitization, will be needed to understand Ca^{2+}-dependent mechanisms of ELKS in controlling RRP.

Outlook

Our experiments reveal that ELKS supports neurotransmitter release at inhibitory synapses via enhancing action potential induced Ca^{2+} entry. Our experiments also raise additional questions.

First, it will be important to determine roles of ELKS at central synapses other than inhibitory hippocampal synapses. Existing data suggest that ELKS has synapse-specific roles. At synapses with prominent dense projections, such as the rod photoreceptor ribbon synapse and the *Drosophila* NMJ, ELKS2, and brp, respectively, operate as scaffolding proteins (Kittel et al., 2006; tom Dieck et al., 2012). At synapses with conventional active zones, such as the *C. elegans* NMJ or mouse hippocampal synapses, loss of ELKS results in more subtle deficits (Deken et al., 2005; Dai et al., 2006; Kaeser et al., 2009; current study). It will be important to test whether enhancing presynaptic Ca^{2+} entry is a universal role of ELKS or whether it is specific to particular synapses. Second, the observation that genetic removal of ELKS1 is embryonically lethal suggests developmental roles for ELKS that are independent of synaptic transmission because neurotransmitter release is not necessary for embryonic survival (Verhage et al., 2000). Brp may have similar roles because mutant flies that only lack the 17 C-terminal amino acids of brp have normal basal neurotransmitter release but show impaired survival and motor activity (Hallermann et al., 2010b). Developmental roles of ELKS could be mediated through Rab6-dependent trafficking (Monier et al., 2002; Grigoriev et al., 2007) or through NF-κB signaling (Ducut Sigala et al., 2004). The mutant mice generated in this study will be invaluable to answer these questions.

References

Ariel P, Ryan TA (2012) New insights into molecular players involved in neurotransmitter release. Physiology 27:15–24. CrossRef Medline

Augustin I, Rosenmund C, Südhof TC, Brose N (1999) Munc13–1 is essential for fusion competence of glutamatergic synaptic vesicles. Nature 400: 457–461. CrossRef Medline

Billings SE, Clarke GL, Nishimune H (2012) ELKS1 and Ca(2+) channel subunit beta4 interact and colocalize at cerebellar synapses. Neuroreport 23:49–54. CrossRef Medline

Cao YQ, Piedras-Rentería ES, Smith GB, Chen G, Harata NC, Tsien RW (2004) Presynaptic Ca^{2+} channels compete for channel type-preferring slots in altered neurotransmission arising from Ca^{2+} channelopathy. Neuron 43:387–400. CrossRef Medline

Catterall WA, Perez-Reyes E, Snutch TP, Striessnig J (2005) International Union of Pharmacology: XLVIII. Nomenclature and structure–function relationships of voltage-gated calcium channels. Pharmacol Rev 57:411–425. CrossRef Medline

Couteaux R, Pécot-Dechavassine M (1970) [Synaptic vesicles and pouches at the level of "active zones" of the neuromuscular junction]. C R Acad Sci Hebd Seances Acad Sci D 271:2346–2349. Medline

Dai Y, Taru H, Deken SL, Grill B, Ackley B, Nonet ML, Jin Y (2006) SYD-2 Liprin-alpha organizes presynaptic active zone formation through ELKS. Nat Neurosci 9:1479–1487. CrossRef Medline

Davydova D, Marini C, King C, Klueva J, Bischof F, Romorini S, Montenegro-Venegas C, Heine M, Schneider R, Schröder MS, Altrock WD, Henneberger C, Rusakov DA, Gundelfinger ED, Fejtova A (2014) Bassoon specifically controls presynaptic P/Q-type Ca(2+) channels via RIM-binding protein. Neuron 82:181–194. CrossRef Medline

Deguchi-Tawarada M, Inoue E, Takao-Rikitsu E, Inoue M, Ohtsuka T, Takai Y (2004) CAST2: identification and characterization of a protein structurally related to the presynaptic cytomatrix protein CAST. Genes Cells 9:15–23. CrossRef Medline

Deken SL, Vincent R, Hadwiger G, Liu Q, Wang ZW, Nonet ML (2005) Redundant localization mechanisms of RIM and ELKS in *Caenorhabditis elegans*. J Neurosci 25:5975–5983. CrossRef Medline

Deng L, Kaeser PS, Xu W, Südhof TC (2011) RIM proteins activate vesicle priming by reversing autoinhibitory homodimerization of Munc13. Neuron 69:317–331. CrossRef Medline

Dodge FA Jr, Rahamimoff R (1967) On the relationship between calcium concentration and the amplitude of the end-plate potential. J Physiol 189:90P–92P. Medline

Dolphin AC (2003) Beta subunits of voltage-gated calcium channels. J Bioenerg Biomembr 35:599–620. CrossRef Medline

Ducut Sigala JL, Bottero V, Young DB, Shevchenko A, Mercurio F, Verma IM (2004) Activation of transcription factor NF-kappaB requires ELKS, an IkappaB kinase regulatory subunit. Science 304:1963–1967. CrossRef Medline

Dymecki SM (1996) Flp recombinase promotes site-specific DNA recombination in embryonic stem cells and transgenic mice. Proc Natl Acad Sci U S A 93:6191–6196. CrossRef Medline

Fernández-Chacón R, Königstorfer A, Gerber SH, Garcia J, Matos MF, Stevens CF, Brose N, Rizo J, Rosenmund C, Südhof TC (2001) Synaptotagmin I functions as a calcium regulator of release probability. Nature 410:41–49. CrossRef Medline

Fouquet W, Owald D, Wichmann C, Mertel S, Depner H, Dyba M, Hallermann S, Kittel RJ, Eimer S, Sigrist SJ (2009) Maturation of active zone assembly by *Drosophila* Bruchpilot. J Cell Biol 186:129–145. Medline

Frank T, Rutherford MA, Strenzke N, Neef A, Pangršiè T, Khimich D, Fejtova A, Gundelfinger ED, Liberman MC, Harke B, Bryan KE, Lee A, Egner A, Riedel D, Moser T (2010) Bassoon and the synaptic ribbon organize Ca(2)+ channels and vesicles to add release sites and promote refilling. Neuron 68:724–738. CrossRef Medline

Gracheva EO, Hadwiger G, Nonet ML, Richmond JE (2008) Direct interactions between *C. elegans* RAB-3 and Rim provide a mechanism to target vesicles to the presynaptic density. Neurosci Lett 444:137–142. CrossRef Medline

Grigoriev I, Splinter D, Keijzer N, Wulf PS, Demmers J, Ohtsuka T, Modesti M, Maly IV, Grosveld F, Hoogenraad CC, Akhmanova A (2007) Rab6 regulates transport and targeting of exocytotic carriers. Dev Cell 13:305–314. CrossRef Medline

Grigoriev I, Yu KL, Martinez-Sanchez E, Serra-Marques A, Smal I, Meijering E, Demmers J, Peränen J, Pasterkamp RJ, van der Sluijs P, Hoogenraad CC, Akhmanova A (2011) Rab6, Rab8, and MICAL3 cooperate in controlling docking and fusion of exocytotic carriers. Curr Biol 21:967–974. CrossRef Medline

Gundelfinger ED, Fejtova A (2012) Molecular organization and plasticity of the cytomatrix at the active zone. Curr Opin Neurobiol 22:423–430. CrossRef Medline

Hallermann S, Heckmann M, Kittel RJ (2010a) Mechanisms of short-term plasticity at neuromuscular active zones of *Drosophila*. HFSP J 4:72–84. CrossRef Medline

Hallermann S, Kittel RJ, Wichmann C, Weyhersmüller A, Fouquet W, Mertel S, Owald D, Eimer S, Depner H, Schwärzel M, Sigrist SJ, Heckmann M (2010b) Naked dense bodies provoke depression. J Neurosci 30:14340–14345. CrossRef Medline

Han Y, Kaeser PS, Südhof TC, Schneggenburger R (2011) RIM determines Ca(2+) channel density and vesicle docking at the presynaptic active zone. Neuron 69:304–316. CrossRef Medline

Harlow ML, Ress D, Stoschek A, Marshall RM, McMahan UJ (2001) The architecture of active zone material at the frog's neuromuscular junction. Nature 409:479–484. CrossRef Medline

Hibino H, Pironkova R, Onwumere O, Vologodskaia M, Hudspeth AJ, Lesage F (2002) RIM binding proteins (RBPs) couple Rab3-interacting molecules (RIMs) to voltage-gated Ca(2+) channels. Neuron 34:411–423. CrossRef Medline

Ho A, Morishita W, Atasoy D, Liu X, Tabuchi K, Hammer RE, Malenka RC, Südhof TC (2006) Genetic analysis of Mint/X11 proteins: essential presynaptic functions of a neuronal adaptor protein family. J Neurosci 26:13089–13101. CrossRef Medline

Hosaka M, Südhof TC (1999) Homo- and heterodimerization of synapsins. J Biol Chem 274:16747–16753. CrossRef Medline

Juranek J, Mukherjee K, Rickmann M, Martens H, Calka J, Südhof TC, Jahn R (2006) Differential expression of active zone proteins in neuromuscular junctions suggests functional diversification. Eur J Neurosci 24:3043–3052. CrossRef Medline

Kaeser PS (2011) Pushing synaptic vesicles over the RIM. Cell Logist 1:106–110. CrossRef Medline

Kaeser PS, Regehr WG (2014) Molecular mechanisms for synchronous, asynchronous, and spontaneous neurotransmitter release. Annu Rev Physiol 76:333–363. CrossRef Medline

Kaeser PS, Kwon HB, Chiu CQ, Deng L, Castillo PE, Südhof TC (2008) RIM1alpha and RIM1beta are synthesized from distinct promoters of the RIM1 gene to mediate differential but overlapping synaptic functions. J Neurosci 28:13435–13447. CrossRef Medline

Kaeser PS, Deng L, Chávez AE, Liu X, Castillo PE, Südhof TC (2009) ELKS2alpha/CAST deletion selectively increases neurotransmitter release at inhibitory synapses. Neuron 64:227–239. CrossRef Medline

Kaeser PS, Deng L, Wang Y, Dulubova I, Liu X, Rizo J, Südhof TC (2011) RIM proteins tether Ca^{2+} channels to presynaptic active zones via a direct PDZ–domain interaction. Cell 144:282–295. CrossRef Medline

Kaeser PS, Deng L, Fan M, Südhof TC (2012) RIM genes differentially contribute to organizing presynaptic release sites. Proc Natl Acad Sci U S A 109:11830–11835. CrossRef Medline

Kaufman DL, Houser CR, Tobin AJ (1991) Two forms of the gamma-aminobutyric acid synthetic enzyme glutamate decarboxylase have distinct intraneuronal distributions and cofactor interactions. J Neurochem 56:720–723. CrossRef Medline

Kittel RJ, Wichmann C, Rasse TM, Fouquet W, Schmidt M, Schmid A, Wagh DA, Pawlu C, Kellner RR, Willig KI, Hell SW, Buchner E, Heckmann M, Sigrist SJ (2006) Bruchpilot promotes active zone assembly, Ca^{2+} channel clustering, and vesicle release. Science 312:1051–1054. CrossRef Medline

Kiyonaka S, Wakamori M, Miki T, Uriu Y, Nonaka M, Bito H, Beedle AM, Mori E, Hara Y, De Waard M, Kanagawa M, Itakura M, Takahashi M, Campbell KP, Mori Y (2007) RIM1 confers sustained activity and neurotransmitter vesicle anchoring to presynaptic Ca^{2+} channels. Nat Neurosci 10:691–701. CrossRef Medline

Kiyonaka S, Nakajima H, Takada Y, Hida Y, Yoshioka T, Hagiwara A, Kitajima I, Mori Y, Ohtsuka T (2012) Physical and functional interaction of the active zone protein CAST/ERC2 and the beta-subunit of the voltage-dependent Ca(2+) channel. J Biochem 152:149–159. CrossRef Medline

Koushika SP, Richmond JE, Hadwiger G, Weimer RM, Jorgensen EM, Nonet ML (2001) A post-docking role for active zone protein Rim. Nat Neurosci 4:997–1005. CrossRef Medline

Lau CG, Murthy VN (2012) Activity-dependent regulation of inhibition via GAD67. J Neurosci 32:8521–8531. CrossRef Medline

Lazarevic V, Schöne C, Heine M, Gundelfinger ED, Fejtova A (2011) Extensive remodeling of the presynaptic cytomatrix upon homeostatic adaptation to network activity silencing. J Neurosci 31:10189–10200. CrossRef Medline

Liu KS, Siebert M, Mertel S, Knoche E, Wegener S, Wichmann C, Matkovic T, Muhammad K, Depner H, Mettke C, Bückers J, Hell SW, Müller M, Davis GW, Schmitz D, Sigrist SJ (2011) RIM-binding protein, a central part of the active zone, is essential for neurotransmitter release. Science 334: 1565–1569. CrossRef Medline

Matkovic T, Siebert M, Knoche E, Depner H, Mertel S, Owald D, Schmidt M, Thomas U, Sickmann A, Kamin D, Hell SW, Bürger J, Hollmann C, Mielke T, Wichmann C, Sigrist SJ (2013) The Bruchpilot cytomatrix determines the size of the readily releasable pool of synaptic vesicles. J Cell Biol 202:667–683. CrossRef Medline

Maximov A, Pang ZP, Tervo DG, Südhof TC (2007) Monitoring synaptic transmission in primary neuronal cultures using local extracellular stimulation. J Neurosci Methods 161:75–87. CrossRef Medline

Monier S, Jollivet F, Janoueix-Lerosey I, Johannes L, Goud B (2002) Characterization of novel Rab6-interacting proteins involved in endosome-to-TGN transport. Traffic 3:289–297. CrossRef Medline

Mozhayeva MG, Sara Y, Liu X, Kavalali ET (2002) Development of vesicle pools during maturation of hippocampal synapses. J Neurosci 22:654–665. Medline

Mukherjee K, Yang X, Gerber SH, Kwon HB, Ho A, Castillo PE, Liu X, Südhof TC (2010) Piccolo and bassoon maintain synaptic vesicle clustering without directly participating in vesicle exocytosis. Proc Natl Acad Sci U S A 107:6504–6509. CrossRef Medline

Müller M, Liu KS, Sigrist SJ, Davis GW (2012) RIM controls homeostatic plasticity through modulation of the readily-releasable vesicle pool. J Neurosci 32:16574–16585. CrossRef Medline

Nakata T, Kitamura Y, Shimizu K, Tanaka S, Fujimori M, Yokoyama S, Ito K, Emi M (1999) Fusion of a novel gene, ELKS, to RET due to translocation t(10;12)(q11;p13) in a papillary thyroid carcinoma. Genes Chromosomes Cancer 25:97–103. CrossRef Medline

Nishimune H, Numata T, Chen J, Aoki Y, Wang Y, Starr MP, Mori Y, Stanford JA (2012) Active zone protein Bassoon co-localizes with presynaptic calcium channel, modifies channel function, and recovers from aging related loss by exercise. PLoS One 7:e38029. CrossRef Medline

O'Gorman S, Dagenais NA, Qian M, Marchuk Y (1997) Protamine-Cre recombinase transgenes efficiently recombine target sequences in the male germ line of mice, but not in embryonic stem cells. Proc Natl Acad Sci U S A 94:14602–14607. CrossRef Medline

Ohtsuka T, Takao-Rikitsu E, Inoue E, Inoue M, Takeuchi M, Matsubara K, Deguchi-Tawarada M, Satoh K, Morimoto K, Nakanishi H, Takai Y (2002) Cast: a novel protein of the cytomatrix at the active zone of synapses that forms a ternary complex with RIM1 and munc13-1. J Cell Biol 158:577–590. CrossRef Medline

Rosahl TW, Geppert M, Spillane D, Herz J, Hammer RE, Malenka RC, Südhof TC (1993) Short-term synaptic plasticity is altered in mice lacking synapsin I. Cell 75:661–670. CrossRef Medline

Rosenmund C, Stevens CF (1996) Definition of the readily releasable pool of vesicles at hippocampal synapses. Neuron 16:1197–1207. CrossRef Medline

Rosenmund C, Sigler A, Augustin I, Reim K, Brose N, Rhee JS (2002) Differential control of vesicle priming and short-term plasticity by Munc13 isoforms. Neuron 33:411–424. CrossRef Medline

Schoch S, Castillo PE, Jo T, Mukherjee K, Geppert M, Wang Y, Schmitz F, Malenka RC, Südhof TC (2002) RIM1alpha forms a protein scaffold for regulating neurotransmitter release at the active zone. Nature 415:321–326. CrossRef Medline

Schoch S, Mittelstaedt T, Kaeser PS, Padgett D, Feldmann N, Chevaleyre V, Castillo PE, Hammer RE, Han W, Schmitz F, Lin W, Südhof TC (2006) Redundant functions of RIM1alpha and RIM2alpha in Ca(2+)-triggered neurotransmitter release. EMBO J 25:5852–5863. CrossRef Medline

Sorensen JB, Fernández-Chacón R, Südhof TC, Neher E (2003) Examining synaptotagmin 1 function in dense core vesicle exocytosis under direct control of Ca^{2+}. J Gen Physiol 122:265–276. CrossRef Medline

Südhof TC (2012) The presynaptic active zone. Neuron 75:11–25. CrossRef Medline

Sun J, Pang ZP, Qin D, Fahim AT, Adachi R, Südhof TC (2007) A dual-Ca^{2+}-sensor model for neurotransmitter release in a central synapse. Nature 450:676–682. CrossRef Medline

tom Dieck S, Specht D, Strenzke N, Hida Y, Krishnamoorthy V, Schmidt KF, Inoue E, Ishizaki H, Tanaka-Okamoto M, Miyoshi J, Hagiwara A, Brandstätter JH, Löwel S, Gollisch T, Ohtsuka T, Moser T (2012) Deletion of the presynaptic scaffold CAST reduces active zone size in rod photoreceptors and impairs visual processing. J Neurosci 32:12192–12203. CrossRef Medline

Verhage M, Maia AS, Plomp JJ, Brussaard AB, Heeroma JH, Vermeer H, Toonen RF, Hammer RE, van den Berg TK, Missler M, Geuze HJ, Südhof TC (2000) Synaptic assembly of the brain in the absence of neurotransmitter secretion. Science 287:864–869. CrossRef Medline

Wagh DA, Rasse TM, Asan E, Hofbauer A, Schwenkert I, Dürrbeck H, Buchner S, Dabauvalle MC, Schmidt M, Qin G, Wichmann C, Kittel R, Sigrist SJ, Buchner E (2006) Bruchpilot, a protein with homology to ELKS/CAST, is required for structural integrity and function of synaptic active zones in *Drosophila*. Neuron 49:833–844. CrossRef Medline

Wang Y, Liu X, Biederer T, Südhof TC (2002) A family of RIM-binding proteins regulated by alternative splicing: implications for the genesis of synaptic active zones. Proc Natl Acad Sci U S A 99:14464–14469. CrossRef Medline

Weimer RM, Gracheva EO, Meyrignac O, Miller KG, Richmond JE, Bessereau JL (2006) UNC-13 and UNC-10/rim localize synaptic vesicles to specific membrane domains. J Neurosci 26:8040–8047. CrossRef Medline